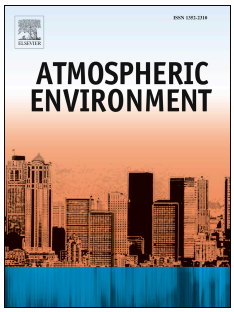
Journal Pre-proof



The dust load and radiative impact associated with the June 2020 historical Saharan dust storm

Diana Francis, Narendra Nelli, Ricardo Fonseca, Michael Weston, Cyrille Flamant, Charfeddine Cherif

PII: S1352-2310(21)00630-0

DOI: https://doi.org/10.1016/j.atmosenv.2021.118808

Reference: AEA 118808

To appear in: *Atmospheric Environment*

Received Date: 28 May 2021

Revised Date: 19 October 2021

Accepted Date: 20 October 2021

Please cite this article as: Francis, D., Nelli, N., Fonseca, R., Weston, M., Flamant, C., Cherif, C., The dust load and radiative impact associated with the June 2020 historical Saharan dust storm, *Atmospheric Environment* (2021), doi: https://doi.org/10.1016/j.atmosenv.2021.118808.

This is a PDF file of an article that has undergone enhancements after acceptance, such as the addition of a cover page and metadata, and formatting for readability, but it is not yet the definitive version of record. This version will undergo additional copyediting, typesetting and review before it is published in its final form, but we are providing this version to give early visibility of the article. Please note that, during the production process, errors may be discovered which could affect the content, and all legal disclaimers that apply to the journal pertain.

© 2021 Published by Elsevier Ltd.

Journal Pre-proof

The Dust Load and Radiative Impact associated with the June 2020 historical Saharan Dust Storm

Diana Francis[1*], Narendra Nelli[1], Ricardo Fonseca[1], Michael Weston[1], Cyrille Flamant[2], Charfeddine Cherif[1]

[1] Environmental and Geophysical Sciences Lab, Khalifa University, P.O. Box 127788, Abu Dhabi, UAE.

[2] CNRS and UVSQ, LATMOS, Sorbonne Universités, 75005 Paris, France.

Corresponding Author: diana.francis@ku.ac.ae

Credit Author Statement:

Diana Francis: Conceptualization, Methodology, Investigation, supervision, Original draft preparation and Reviewing.

Narendra Nelli: Visualization, data curation and analysis.

Ricardo Fonseca: Formal analysis, Validation, Writing - Original draft preparation and Reviewing.

Michael Weston: Performance of WRF model simulations and analysis.

Cyrille Flamant: Analysis and validation.

Charfeddine Cherif: Software, Data curation.

Journal Pre-proof

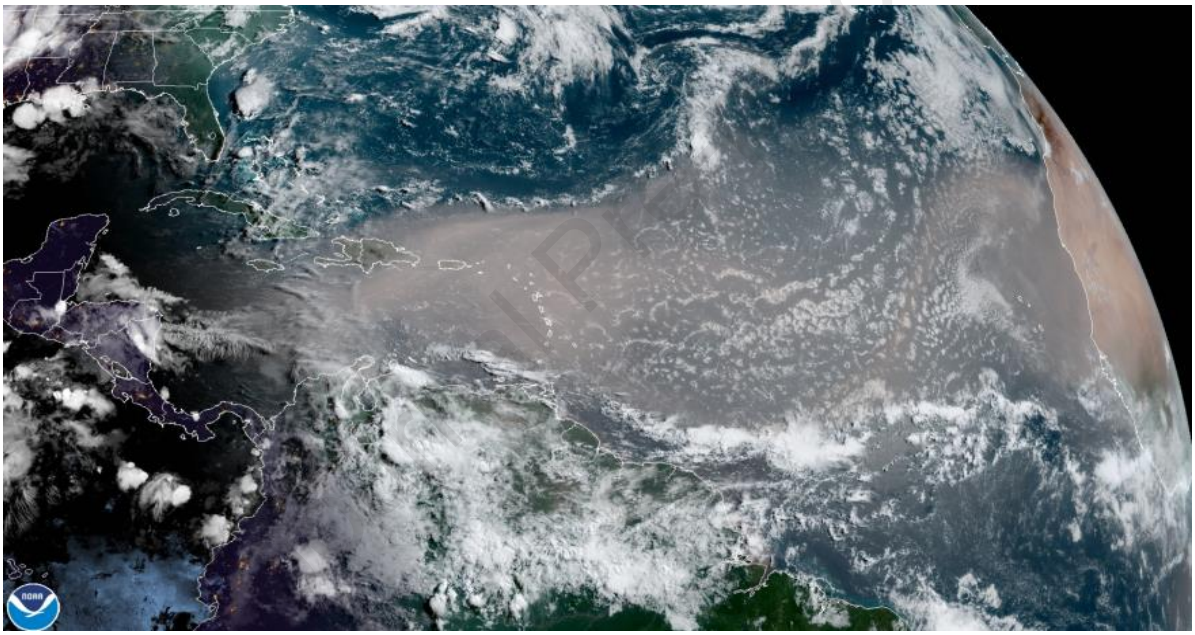
The Dust Load and Radiative Impact associated with the June 2020 historical Saharan Dust Storm

Diana Francis[1*], Narendra Nelli[1], Ricardo Fonseca[1], Michael Weston[1], Cyrille Flamant[2], Charfeddine Cherif[1]

[1] Environmental and Geophysical Sciences Lab, Khalifa University, P.O. Box 127788, Abu Dhabi, UAE.

[2] CNRS and UVSQ, LATMOS, Sorbonne Universités, 75005 Paris, France.

Corresponding Author: diana.francis@ku.ac.ae



The Saharan dust storm in June 2020 over the Atlantic Ocean heading to the Caribbean. Image Credit: NOAA.

Dust is an important component of the Earth's atmosphere, with a wide range of impacts ranging from human health to effects on the ocean and climate. In fact, airborne dust aerosols modify the energy budget of the Earth's surface by interacting with the solar radiation in different ways where they absorb in the ultraviolet and longwave and reflect in the shortwave. In June 2020, massive amounts of dust were lifted from the Sahara, the major dust source region in the world, and transported all the way into the Americas across the tropical Atlantic Ocean. During this event, large dust loads, in excess of 8 Tg, covered the tropical Atlantic Ocean and induced a radiative forcing at the surface. The energy budget of the atmosphere and the ocean surface was impacted during this event resulting in a sustained warming during night and a cooling during day. The resulting effect of dust during this event was an increase in the air temperature and the sea surface temperature associated with an increase in the longwave radiation especially during night due to the re-emission of radiation towards the surface by the dust clouds. This warming may have contributed to the very active tropical storms' season in summer 2020.

Journal Pre-proof

The Dust Load and Radiative Impact associated with the June 2020 historical Saharan Dust Storm

Diana Francis[1*], Narendra Nelli[1], Ricardo Fonseca[1], Michael Weston[1], Cyrille Flamant[2], Charfeddine Cherif[1]

[1] Environmental and Geophysical Sciences Lab, Khalifa University, P.O. Box 127788, Abu Dhabi, UAE.

[2] CNRS and UVSQ, LATMOS, Sorbonne Universités, 75005 Paris, France.

Corresponding Author: diana.francis@ku.ac.ae

Highlights:

- June 2020 Saharan dust storm associated with highest-on-record aerosol optical depths;
- The estimated dust loads exceeded 8 Tg over the eastern tropical Atlantic;
- The dust event caused a net warming of the ocean surface by up to 1.1 K;
- Dust may have contributed to the extremely active 2020 Atlantic hurricane season.

Abstract

In June 2020, a major dust outbreak occurred in the Sahara that impacted the tropical Atlantic Ocean. In this study, the dust load and radiative forcing of the dust plumes on both the atmosphere and ocean surface is investigated by means of observations and modelling. We estimated dust loadings in excess of 8 Tg over the eastern tropical Atlantic, comparable to those observed over the desert during major Saharan dust storms. The dust induced an up to 1.1 K net warming of the ocean surface and a 1.8K warming of the air temperature (i.e., two to three times the respective climatological standard deviations), with a +14 W m^{-2} (~28% of the mean value) increase in the surface net radiation flux at night. As the dust plumes extended all the way to the Caribbean, it is possible that this historical dust event helped fuel the record-breaking 2020 Atlantic hurricane season.

Keywords: Dust aerosols, radiative forcing, Sahara, Tropical Atlantic, WRF-Chem.

Journal Pre-proof

1. Introduction

Aerosols have a profound impact on the surface and atmospheric energy budgets, owing to their interaction with the radiation and cloud microphysics (e.g., Haywood and Boucher, 2000; Satheesh and Moorthy, 2005). The most abundant aerosol type on Earth is mineral dust, with the Sahara Desert its major source (Kok et al., 2021). Dust has an important impact on the climate system (e.g., Choobari et al., 2014). For example, its accurate representation has been shown to help in the simulation of the tropical/monsoon precipitation (e.g., Zhao et al., 2011; Balkanski et al., 2021), hurricanes and tropical storms (e.g., Chen et al., 2017), local and regional weather conditions (e.g., Spyrou et al., 2013; Weston et al., 2020; Francis et al., 2020a), and ocean dynamics (e.g., Evan et al., 2012). Furthermore, mineral dust is known to strongly influence the radiative budget due to its significant scattering, absorbing and re-emitting properties (Haywood et al., 2005; Prakash et al., 2015; Di Bagio et al., 2017). By virtue of their distinctive optical properties, mineral dust aerosols scatter and absorb shortwave (SW) and absorb and re-emit longwave (LW) radiation (e.g., Sokolik et al., 2001; Dubovik et al., 2006), therefore modifying the atmospheric thermodynamics and regional atmospheric circulations (e.g., Heald et al., 2014; Francis et al., 2020a). Besides the aforementioned surface and atmospheric changes, dust carries with it pollutants, some of which are toxic (e.g. pesticides and herbicides), and microorganisms (e.g. fungi, viruses and bacteria) that can have harmful effects on the fauna and flora (e.g. Griffin et al., 2002). In fact, Azua-Bustos et al. (2019) reported that a number of viable bacteria and fungi can traverse the Atacama Desert unscathed using wind-transported dust, stressing how they can propagate far away from the source region and affect different ecosystems. Dust outbreaks are therefore linked to human health and air quality impacts. When inhaled, the fine dust particles can penetrate deep into the lungs, and the smallest ones even into the alveoli, increasing the risk of cardiopulmonary diseases and leading to premature mortality (Ginnadaki et al., 2014). In addition, the combination of wind and dust reduces visibility, having a pronounced impact on day-to-day activities such as transportation and agriculture (e.g. Al-Hemoud et al., 2017).

By absorbing and scattering solar radiation, dust aerosols reduce the amount of energy reaching the surface (e.g., Kosmopoulos et al., 2017; Jia et al., 2018), which can lead to reduced surface heating and thus latent and sensible heat fluxes (Wang et al., 2004; Prakash et al., 2015; Kaskaoutis et al., 2019). At the same time, dust absorption of both LW and SW radiation can contribute to localized heating by directly warming the dust-laden atmospheric layer (e.g., Weston et al., 2020; Francis et al., 2020a), and enhance the greenhouse effect by re-emitting LW radiation towards the surface (Heinold et al., 2008; Francis et al., 2020a). In all cases, the intensity of the radiative impact of dust in both SW and LW depends strongly on the location of the dust layer in altitude (e.g., Saleeby et al., 2019), and whether it's over water, vegetated areas or desert lands (e.g., Wang et al., 2013). Over the last few decades, dust aerosols have been thought to induce a net cooling at the surface and contribute to the decrease in tropical storm activity over the tropical Atlantic (e.g., Evan et al., 2006). However, recent studies found that the warming effect of dust aerosols has been previously underpredicted due to the underestimation of the amount of large particles in the

atmosphere (e.g., Adebiyi and Kok, 2020), and the misrepresentation of their effect in the LW radiation (Francis et al., 2020a).

One of the most daunting challenges in our understanding of dust and its impacts on the climate system is the quantification of the dust net radiative effect (DRE; Sokolik et al., 2001) accounting for both SW and LW interactions. This remains challenging mainly because of the lack of observations at large scale and of a full understanding of the complexity of the processes involved as well as the feedback among them. In addition, the DRE is highly dependent on dust properties, such as size, shape and composition (Wang et al., 2006; Rontu et al., 2020; Ito et al., 2021). In this case, the use of modelling approaches is common where the DRE can be estimated using the observed dust properties and a radiative transfer model, or through coupled atmospheric-chemistry models such as the Weather Research and Forecasting - Chemistry (WRF-Chem; Grell et al., 2005) model, which is the case in this study. WRF-CHEM has been found to exhibit reasonable skill in simulating dust storms and the direct effect of dust aerosols (e.g., Liu et al., 2016; Singh et al., 2021), including over North Africa (e.g., Teixeira et al., 2016; Flaounas et al., 2017).

Haywood et al. (2003) and Highwood et al. (2003) examined the DRE of a mineral dust storm off the coast of Africa in the year 2000 during the Saharan Dust Experiment (SHADE) measurement campaign (Tanre et al., 2003). They measured a peak SW DRE of up to -130 $W m^{-2}$ (Haywood et al., 2003) and a corresponding LW DRE of around +7 $W m^{-2}$ at the surface (Highwood et al., 2003). This indicates that, for clear sky conditions over the ocean, the reduction in SW radiation flux exceeds in magnitude the increase in LW flux, in line with the findings of other studies (e.g., Slingo et al., 2006). For the same field campaign, Myhre et al. (2003) reported Aerosol Optical Depths (AODs), an indication of the attenuation of the incoming SW radiation due to the presence of aerosols, in excess of 1.5 at the offshore Cape Verde Islands on 26 September, when the modelled net radiative impact of the mineral dust over the eastern tropical Atlantic peaked at around -110 $W m^{-2}$. Even far away from the source region Saharan dust can have a pronounced radiative impact. For example, Gutleben et al. (2020), and in the vicinity of Barbados in the Caribbean, estimated maximum SW radiative effects of -40 $W m^{-2}$ (at the surface) and -25 $W m^{-2}$ (at the TOA) for a dust event in August 2016, when the AOD exceeded 0.3. A comparable variation of the radiation fluxes, but for the daily-mean values, was noted by Kaskaoutis et al. (2019) for a dust storm in Greece in March 2018, when AODs higher than 4 were observed. Dust storms have repeatedly impacted the entire Mediterranean Basin, spanning from the Iberian Peninsula on the western side (e.g. Anton et al., 2014) to Cyprus on the eastern side (e.g. Uzan et al., 2018). For a dust storm in southeastern Spain on 06 September 2007, Anton et al. (2014) noted that, for a one unit increase in the AOD at 675 nm, the SW irradiance at the surface decreased by 187 W m^{-2} and the LW irradiance increased by 20 W m^{-2} (the observed AOD was in the range 0.8 to 1.5). Therefore, as the dust loading goes up, the offset of the decrease in the SW irradiance by the increase in the LW irradiance becomes smaller, dropping from 40% for an AOD of 0.8 to 20% for an AOD of 1.5. A very severe dust storm affected the eastern Mediterranean in September

2015, with AODs at 550 nm exceeding 5 in Cyprus (Solomos et al., 2017), and extended into the Middle East (Francis et al., 2019). Surface radiation measurements in northern Israel revealed a roughly 600 W m^{-2} drop in the global solar radiation in association with the event, with dust layers up to 5 km (Uzan et al., 2018).

Saidou Chaibou et al. (2020) investigated the DRE over western Africa and its impact on the surface and TOA energy budget during summer 2006. The DRE is estimated by taking the difference between a simulation in which the dust radiative effects are considered and one where the radiative impacts are not activated. The DRE at the TOA is positive over the Sahara Desert and negative over the Gulf of Guinea and vegetated areas, with a mean value of +9 W m^{-2}. On the other hand, the mean DRE at the surface is -13 W m^{-2}, reflecting the cooling by dust aerosols. In addition to its impact on the SW and LW fluxes, dust aerosols also affect the other terms of the surface energy budget: e.g. the sensible heat flux (SHF) is cut by up to 24 W m^{-2}, owing to a colder surface by up to 2ºC, while the latent heat flux (LHF) increases up to 12 W m^{-2} over the desert (evaporation) and is lower by up to 24 W m^{-2} over the vegetated regions further south. What is more, the DRE also exhibits a clear diurnal cycle, as the SW radiation flux is only non-zero during daytime meaning that, at night, the LW radiation flux will balance the heat fluxes and ground heat flux (Nelli et al., 2020).

A recent record-breaking Saharan dust storm took place in mid-June 2020. As detailed in Francis et al. (2020b), this event was triggered by a pressure dipole over northwestern Africa, with a ridge, associated with a circum-global wavetrain, just to the west of the Saharan heat low. This dipole led to persistent northeasterly winds and continuous dust emissions over a 4-day period. While the mechanisms behind the observed event are discussed in detail in Francis et al. (2020b), no attempt has been made to quantify the lifted dust and its radiative impact. This will be addressed in the present paper. The goal of this study is twofold: (i) estimate the amount of dust aerosols emitted during the event and compare it to dust emissions available in the literature; (ii) estimate the DRE over the Atlantic Ocean during the event, and speculate on its implications in particular on the tropical cyclone activity, as the eastern tropical Atlantic around the Cape Verde islands, the target region in this study, is a primary breeding area for Atlantic hurricanes (e.g. Haggard, 1958). The findings of this work will help to better understand the effects of dust on the climate system, in particular as major dust storms, such as the June 2020 Saharan dust storm, may become more frequent in a warming climate (e.g., Bellouin et al., 2020).

This paper is structured as follows. In section 2, a summary of the observational and modelling products used in this study is given. The experimental set up of WRF-CHEM is also described. The dust load and DRE estimates and their implications are discussed in section 3, while in section 4 the main findings are outlined.

2. Data and methods

2.1 Observational & Reanalysis Datasets

Five observational datasets are used in this work, four of which are satellite-derived products while the last one comprises ground-based measurements.

- Red-Green-Blue (RGB) satellite images from the Spinning Enhanced Visible and Infrared Imager (SEVIRI; Schmetz et al., 2002) instrument on board the Meteosat Second Generation Spacecraft, from 17 to 24 June 2020 (0.05º; 15-min). These images are constructed using the brightness temperatures measured at the 8.7, 10.8, and 12 μm infrared channels (Martinez et al., 2009);
- AOD estimates from the (i) Visible Infrared Imaging Radiometer Suite (VIIRS; Miller et al., 2013) instrument onboard the Suomi National Polar-orbiting Partnership satellite (6 km; hourly), and (ii) the Moderate Resolution Imaging Spectroradiometer (MODIS; Kaufman et al. 1997) instrument on board the Terra and Aqua satellites (1 km; daily). The MODIS products MOD04_L2 and MYD04_L2, algorithm version 6 and level 2 data, are used (Levy and Hsu, 2015a,b). ;
- Clouds and the Earth's Radiant Energy System (CERES; Doelling et al., 2013, 2016; 1º and hourly) surface SW, LW and net radiation fluxes derived from satellite estimates;
- The Group of High-Resolution Sea Surface Temperature (GHRSST; Martin et al., 2012) Level 4 data provides foundation SSTs from a combination of different satellite measurements (0.01º; daily);
- The Aerosol Robotic Network (AERONET; Holben et al., 1998) is a network of ground-based sun photometers that provide 15-min estimates of the AOD at wavelengths in the range 340 to 1640 nm.

Regarding the satellite-derived AOD estimates, it is important to note that, while MODIS' AOD is closer to that estimated using ground-based assets when compared to that given by VIIRS, in particular in desert regions, it has more gaps than the latter (Wang et al. 2017, 2020), and hence the two are used in this study. What is more, the agreement between MODIS AOD and that given AERONET's sun photometers is not always optimal. As noted e.g. by Levy et al. (2005), over land, and in particular in the blue wavelength, MODIS AOD tends to be higher in cleaner environments and lower in dustier environments when compared with ground-based estimates. This likely arises because of an incorrect setting of the surface albedo in the lookup tables. Other sources of error include sub-pixel cloud, snow/ice and water contamination (Chu et al., 2002), as well as varying aerosol properties such as shape (Remer et al., 2005).

In addition to the datasets listed above, ERA-5 (Hersbach et al., 2020) and the Modern-Era Retrospective analysis for Research and Applications version 2 (MERRA-2; Gelaro et al., 2017) reanalysis data are considered. ERA-5 data is available at 0.25º x 0.25º on an hourly basis from 1979 to present, and has the highest spatial and temporal resolution of any publicly available

reanalysis dataset at the time of writing of the paper. MERRA-2 is unique in the sense that it represents aerosols and their interactions with the climate system, allowing for explicit predictions of the AOD and column dust mass loading, which are available at 0.625º x 0.5º and 1-hour resolution.

2.2 WRF-CHEM Simulations

Dust emissions and transport were simulated using WRF-Chem v3.9.1.1 (Grell et al., 2005, Skamarock et al., 2008). A single domain, which covered most of North Africa and adjacent Atlantic Ocean (38.58°W-41.58°E; 1.35°N-37.63°N) at 12 km resolution was used, with 45 vertical levels. Simulations were forced with the 6-hourly National Centers for Environmental Prediction (NCEP) Global Forecast System (GFS; NCEP, 2015) 0.25° x 0.25° data. A summary of the model configuration is presented in Table 1.

In the model simulations, aerosol-radiation feedbacks are accounted for, while aerosol-cloud interactions (i.e. aerosol indirect effects) are not activated. What is more, WRF-Chem is run with dust emissions only, the gas-phase chemistry is not considered. In order to assess the impact of dust aerosols on the radiation budget and atmospheric flow, similar simulations were run without dust, with all other settings remaining unchanged. These two sets of model runs are labelled as "WRF Dust" and "WRF No Dust" throughout the manuscript.

Dust emissions in the model are controlled by the Air Force Weather Agency (AFWA) dust scheme described by Legrand et al. (2018). This scheme uses the erodibility map developed by Ginoux et al (2001) to represent the source strength of emissions. A feature of this scheme is that it accounts for dust emission by three mechanisms: aerodynamic lift, saltation bombardment and particle disaggregation (Legrand et al., 2018). Aerodynamic lift is when particles become airborne due to wind shear. A characteristic of this process is that small particles (diameter < 10 μm) remain on the surface due to forces of adhesion and cohesion, while larger particles (10-250 μm) become lofted (e.g. Colarco et al., 2003). The larger particles then return to the surface (saltation bombardment), where the impact causes the smaller particles to overcome the adhesion and become dislodged and lofted. Dust is emitted into the lowest model level and transported from there in 5 size-bins that range from 0.2 to 20 μm. Land cover classes are taken from the United States Geological Survey (USGS) global database (Loveland et al., 2000, Sertel et al., 2010). The default soil texture in WRF is from the State Soil Geographic (STATSGO)/Food and Agriculture Organization (FAO) soil database (Sanchez et al., 2009; Dy and Fung, 2016). At the lower boundary over the ocean, a simple prognostic scheme is employed for the sea surface skin temperature (SSKT), which is essentially controlled by the SSTs from the GFS forcing data. This parameterization scheme, based on Zeng and Beljaars (2005), accounts for the effects of the radiative and heat fluxes, as well as molecular diffusion and turbulent mixing, and allows the model to simulate the diurnal variability in the SSKT and its feedback to the atmosphere.

Parameterization	Scheme
Radiation SW	Rapid Radiative Transfer Model for GCMs (Iacono et al., 2008)
Radiation LW	Rapid Radiative Transfer Model for GCMs (Iacono et al., 2008)
Boundary Layer	Yonsei University Planetary Boundary Layer (Hong et al., 2006)
Cumulus	Grell 3 (Grell and Dvnyi, 2002)
Microphysics	Lin (Lin et al., 1983)
Land Surface Model	NOAH (Tewari et al., 2004)
Surface Layer	Revised MM5 (Jimenez et al., 2012)
Chemistry	WRF Dust Simulation: Goddard Chemistry Aerosol Radiation and Transport simple/no ozone (gas-phase chemistry not activated) WRF No Dust Simulation: Chemistry module switched off
Dust option	Air Force Weather Agency dust scheme (Legrand et al., 2018)
Aerosol- radiation feedback	Active
Aerosol-cloud feedback	Inactive
Aerosol Optics	Volume approximation

Table 1. WRF-Chem physics and chemistry parameterization

As the dust event lasted for more than 5 days it was decided to break up the simulations into shorter periods, with the model initialized at 00 UTC every 48 h from 12 to 22 June 2020. The chemistry variables, which is only dust in this case, from the previous model run are used as input at the start of the subsequent simulation. For each simulation, the first 12 h are discarded as spin up while the following 36 h (i.e. forecast hours +13 to +48) are retained for analyses.

The aerosol optical properties, such as the extinction coefficient, at different wavelengths in the SW and LW portions of the electromagnetic spectrum, including at 550 nm, are calculated for each model level (Barnard et al., 2010). The AOD is calculated in post-processing by integrating the extinction coefficient, which is explicitly predicted by WRF-Chem for each model layer, over all model layers. Hereafter, the 550 nm AOD will be referred to just as AOD for simplicity.

3. Results

3.1 Estimation of Dust Load

As detailed in Francis et al. (2020b), the June 2020 Sahara dust storm was of historic proportions. Not only were record amounts of dust present in the atmosphere (as evidenced e.g. by the highest ever AOD recorded at an AERONET station in Cape Verde), but the associated dust plume reached all the way to North America. The extreme nature of this event can be seen in Fig. 1, which shows RGB composites from SEVIRI from 17 to 24 June during nighttime (01 UTC) and daytime (13 UTC). The dust emissions over the Sahara and the westward propagation of the dust plume (pink shading), aided by an anomalously strong African Easterly Jet, can be clearly seen.

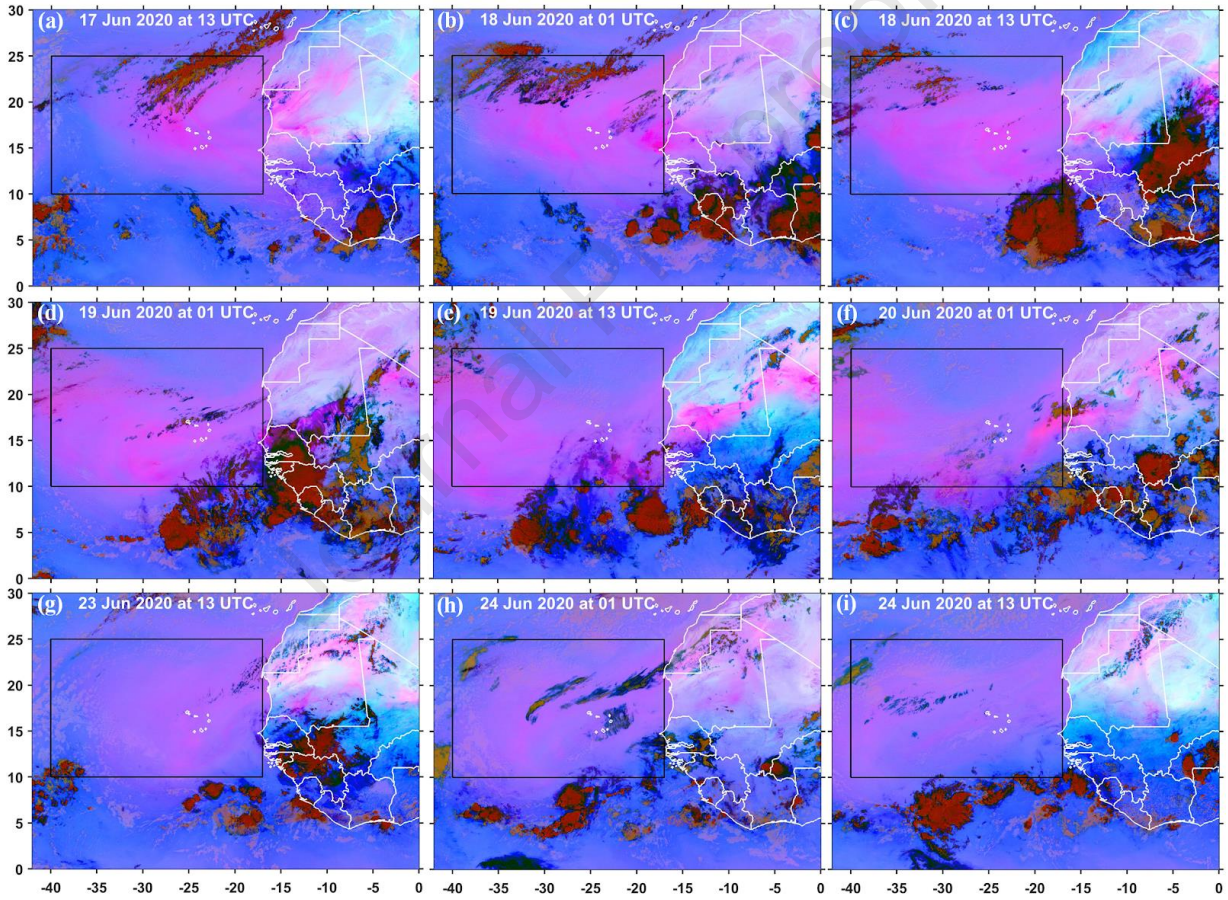


Figure 1. SEVIRI dust RGB snapshots from 17 to 24 June 2020 at 01 UTC (nighttime) and 13 UTC (daytime). In all panels, dust is given in magenta or pink; thick high-level clouds are shaded in orange or brown; thin high-level clouds appear very dark (nearly black); sandy regions are highlighted in white. Dry land is shaded in pale blue during daytime and pale green at night. The region 40ºW-17ºW & 10ºN-25ºN (used for averaging in subsequent figures), which encompasses the bulk of the dust plume at the beginning of the episode, is denoted by a black rectangle.

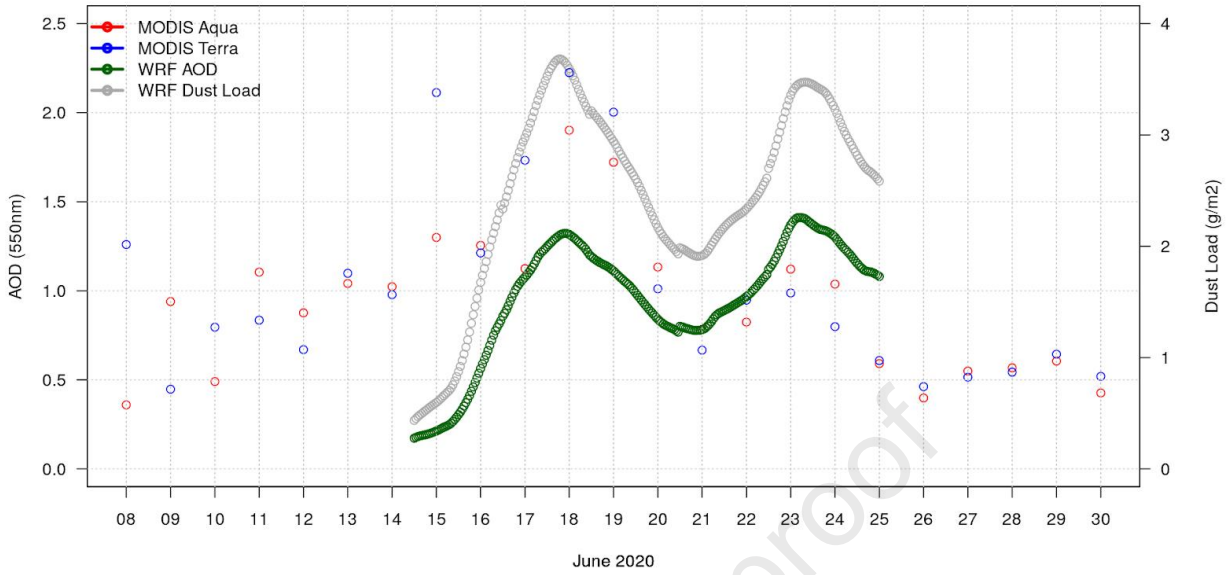
In order to quantify the amount of atmospheric dust, Figure 2 shows WRF and MERRA2-predicted and satellite-derived AOD, as well as modelled column dust mass on 18 June 2020. As

seen in Fig. 1, on this day a dust plume was located over the eastern tropical Atlantic around Cape Verde. AOD estimates exceeded ~2 from MODIS (Fig. 2a) and were as high as ~5 from VIIRS (Fig. 2b). Such high values of AOD are not unheard of (e.g. Solomos et al. (2018) and Kaskaoutis et al. (2019) estimated AODs as high as ~6 during dust storms over the eastern Mediterranean), but have not been observed before in the eastern tropical Atlantic (at least in the Cape Verde Islands), as noted by Francis et al. (2020b). Having said that, it is perfectly possible that, in particularly dusty conditions, such as during haboobs when the Sun can be completely obscured, higher values of AOD have been observed. However, the retrieval algorithm likely flagged the correspondent pixels as cloudy, meaning that such the AOD values are not reported in the literature.

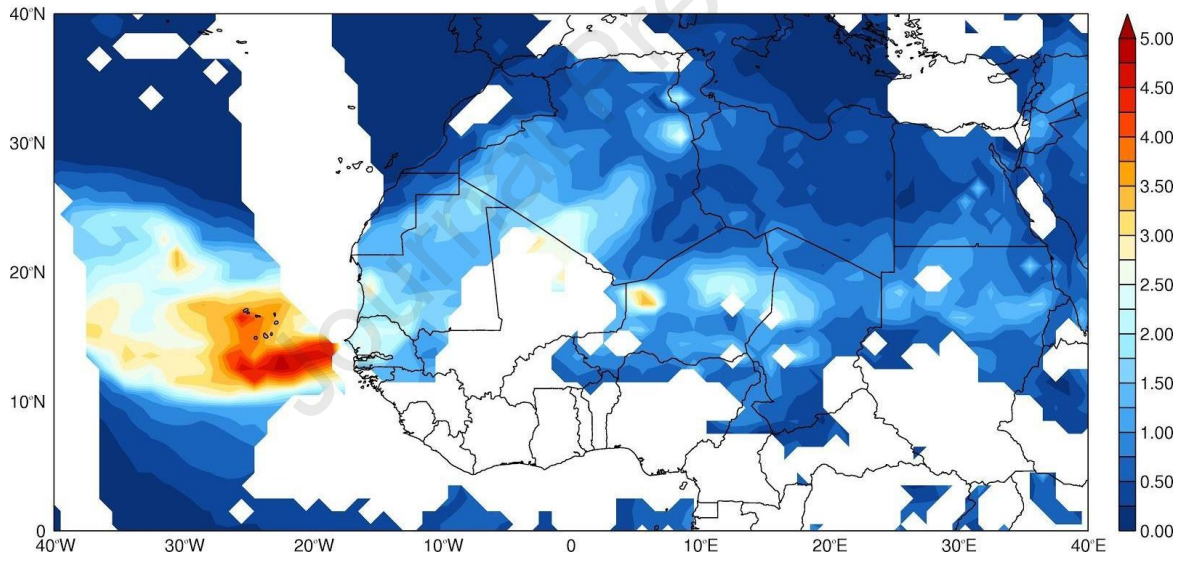
A comparison between the AOD from VIIRS (Fig. 2b) and that of MERRA-2 (Fig. 2d) indicates a similar spatial pattern, even though MERRA-2 underestimates its magnitude. As noted by Buchard et al. (2017), the assimilation of space-based observations of aerosols in the reanalysis data does not correct for all the AOD biases, which are caused e.g. by missing emissions and/or deficiencies in the parameterization schemes. The reanalysis data predicts more than $6\,g\,m^{-2}$ of dust over the tropical eastern Atlantic, with a maximum in the surface dust mass concentration of ~1200 $\mu g\,m^{-3}$. A comparison with other major dust storms revealed that this last figure is roughly (i) 30 times larger than that measured in Puerto Rico during the Sahara dust storm of March 2004 (Rodriguez-Cotto et al., 2013); (ii) four times higher than that observed in the Middle East during six frontal dust storms in 2016-2018 (Hamzeh et al., 2021); (iii) up to 10 times larger than that measured during a major dust storm in East Asia in April 2001 (Manktelow et al., 2010); and (iv) comparable to the amount of dust emitted during major dust storms in the eastern Mediterranean, where several studies reported surface dust concentrations of up to $6000\,\mu g\,m^{-3}$ (Albert and Ganor, 2001; Saeed et al., 2014; Solomos et al., 2018; Kaskaoutis et al., 2019).

(a)

Journal Pre-proof

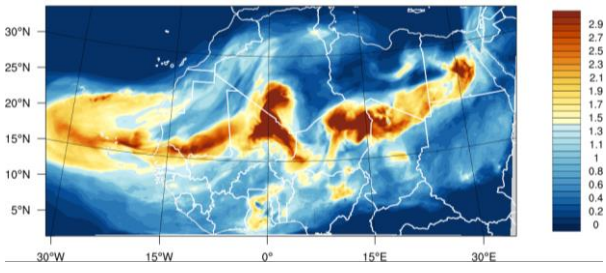


(b)

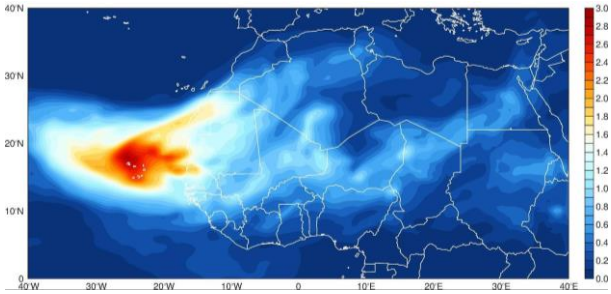


(c)

(d)



(e)



(f)

Journal Pre-proof

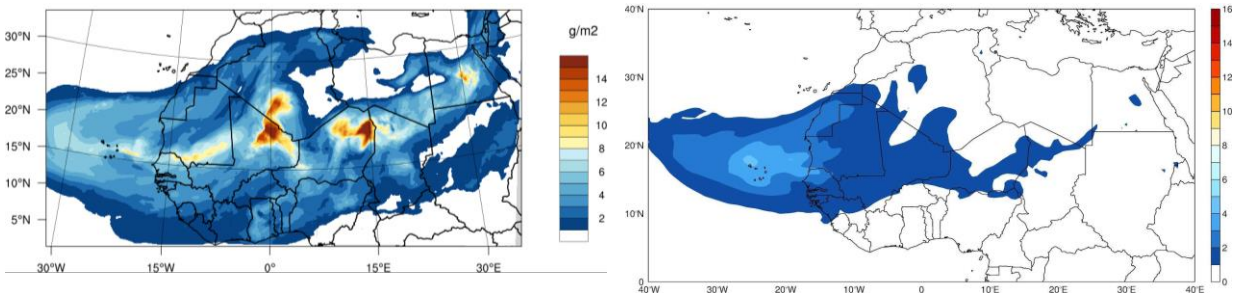
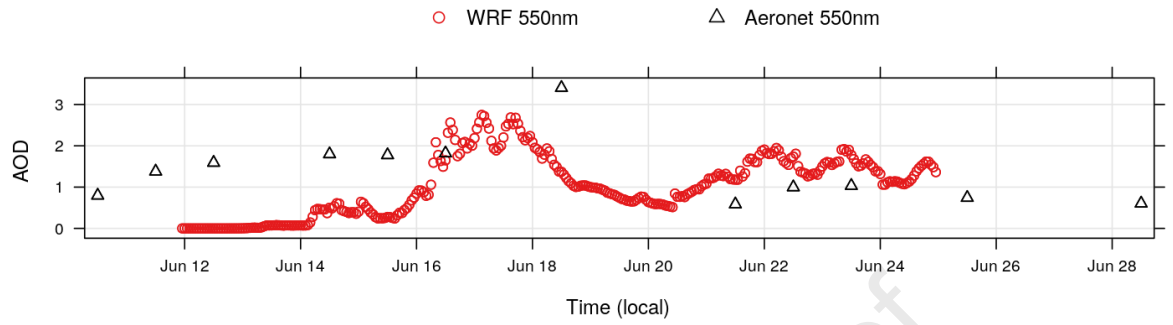


Figure 2 (a) WRF AOD (green circles, left axis) and dust load (grey circles, right axis; g m^{-2}) and MODIS AOD (blue and red circles; left axis), averaged over the eastern tropical Atlantic Ocean (38ºW-17ºW & 10ºN-25ºN), from 08 to 30 June 2020. Spatial distribution of the AOD over the study region on 18 June 2020 from (b) VIIRS satellite (daily maximum; the white shading denotes gaps in the data coverage), (c) WRF and (d) MERRA-2 at 00 UTC. (e) and (f) are as (c) and (d) but for the total column dust mass (g m^{-2}).

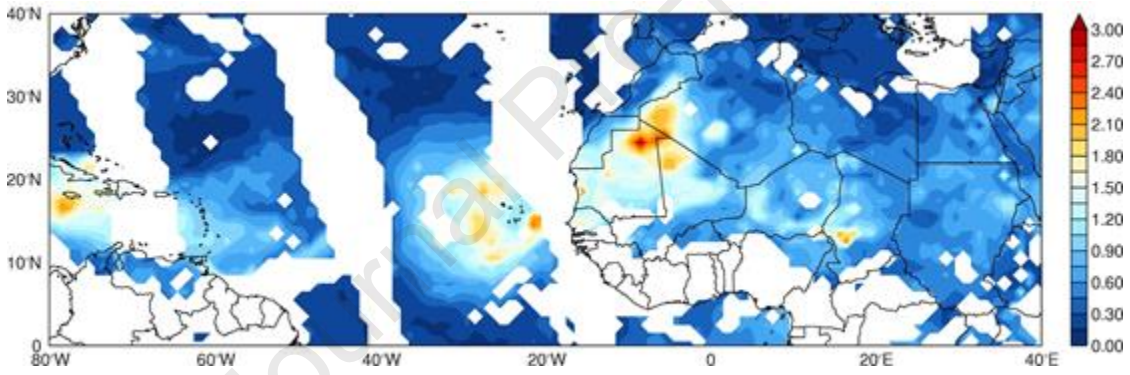
When integrated over the eastern tropical Atlantic (40ºW-17ºW & 10ºN-25ºN; black rectangle in Fig. 1), where the bulk of the dust plume is located, following Todd et al. (2008), the total dust loading is about 7.9 Tg, which is roughly comparable to that estimated over land during other major dust storms (Bou Karam et al. 2009, 2010, 2014; Francis et al., 2020a).

WRF underestimates the observed AOD over the eastern tropical Atlantic on 18 June, on average slightly more than MERRA-2: as seen in Fig. 2a, the WRF-predicted AOD is roughly 0.5-1 lower than that estimated from MODIS and AERONET, respectively. The fact that the atmosphere is less dusty in WRF may be due to (i) uncertainties in the dust parameterization schemes (e.g., Flaounas et al., 2017; Eltahan et al., 2018), which is also the case for MERRA-2; an incorrect representation of the (ii) large-scale circulation (e.g., Kabatas et al., 2018), and (iii) surface properties such as the erodibility factor (e.g., Su et al., 2015). The spatial pattern of the AOD in WRF (Fig. 2c) is also different to that of VIIRS (Fig. 2b) and MERRA-2 (Fig. 2d), with the dust being more concentrated over the desert. A possible reason for this is the lack of data assimilation in WRF, which is employed in the reanalysis dataset. However, the "tongue" of higher amounts of dust over northern Mali, and from Niger and northern Chad to central Egypt in WRF is also present in MERRA-2 and VIIRS. In particular over land, WRF predicts higher AODs than MERRA-2 (Fig. 2c-d), which is also reflected in the larger dust masses (Fig. 2e-f). However, over the eastern tropical Atlantic, the two are broadly in agreement. On 23 June (Fig. 3), the day of the second AOD peak, the WRF and observed AODs are more in line with each other (cf. Fig. 2a and Fig. 3a), with the spatial pattern of the AOD and dust loading also being generally similar between WRF and MERRA-2 (Fig. 3c-f), the latter in close agreement with the VIIRS estimates (Fig. 3b). As on 18 June, WRF predicts substantially higher amounts of dust over northwestern Africa compared to MERRA-2, with AODs roughly ~1-2 index units higher and a dust mass typically ~3-5 g m^{-2} larger than that in the reanalysis dataset. Despite this, over the eastern tropical Atlantic, the two continue to be closer to each other (Fig. 3c-f).

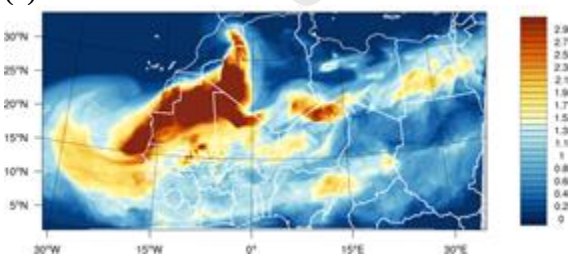
(a)



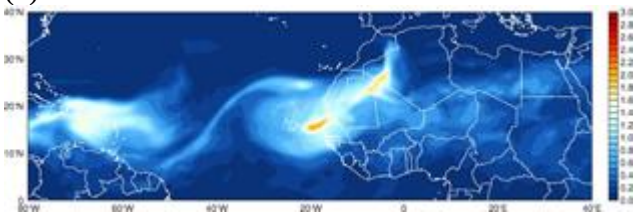
(b)



(c)



(d)



(e)

(f)

Journal Pre-proof

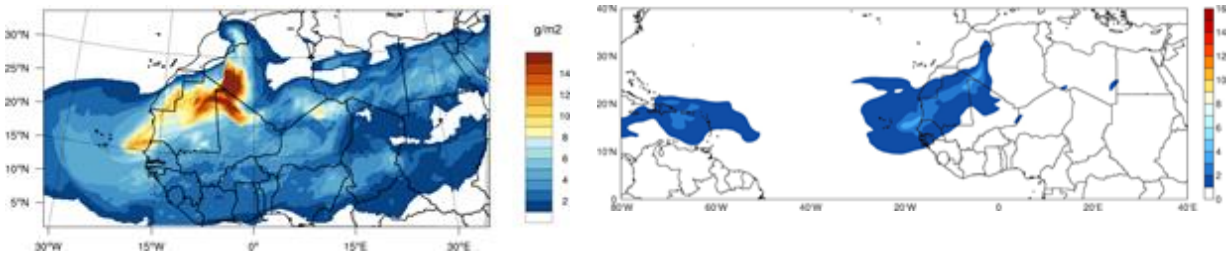
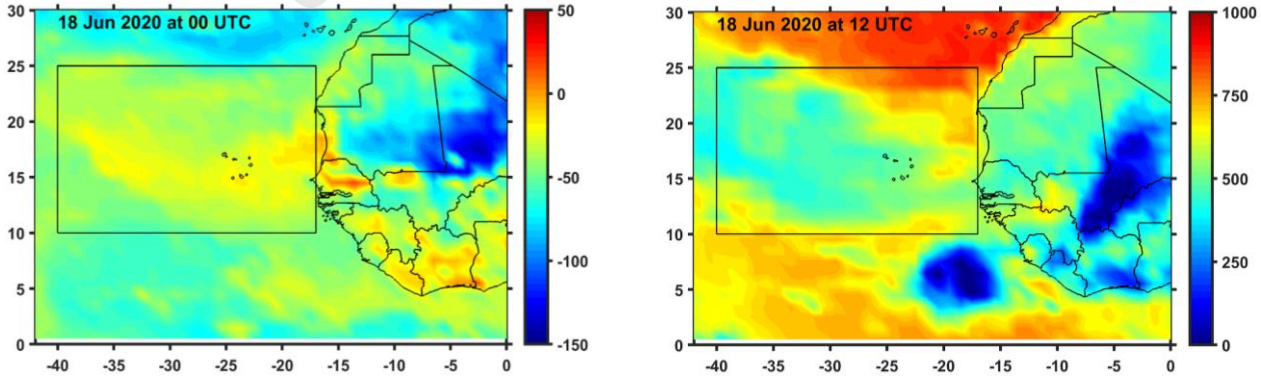


Figure 3 As Figure 2 but on 23 June 2020. In (a), the WRF and observed AOD at 550 nm from 10 to 29 June 2020 are plotted at the location of the AERONET station in Cape Verde (22.935ºW, 16.733ºN). The western boundary in the VIIRS and MERRA-2 plots, panels (b), (d) and (f), is extended to 80ºW, to highlight the propagation of the dust plume into the Caribbean and North America.

3.2 Evaluation of the Dust Radiative Forcing

Dust particles act to block the thermal radiation emitted by the Earth's surface, and scatter and absorb the SW radiation emitted by the Sun (Spyrou et al., 2018). These dust aerosol direct and semi-direct effects can be seen in Figs. 4a-b: the eastern tropical Atlantic, where the dust plume is located, exhibits higher surface net radiation fluxes, R_{net}, at night, when compared to the clearer regions further north around the Canary Islands (~0 W m^{-2}, as opposed to -100 W m^{-2}), and lower during the day (~500 W m^{-2} compared to 800 W m^{-2} further north). The rather low values of R_{net} (<250 W m^{-2}) to the south of the plume and in parts of Mali are due the presence of deep convective clouds (Fig. 1c). The dust effects on R_{net} persisted for several days till the end of June 2020 (Fig. 4c-d).

(a) (b)



Journal Pre-proof

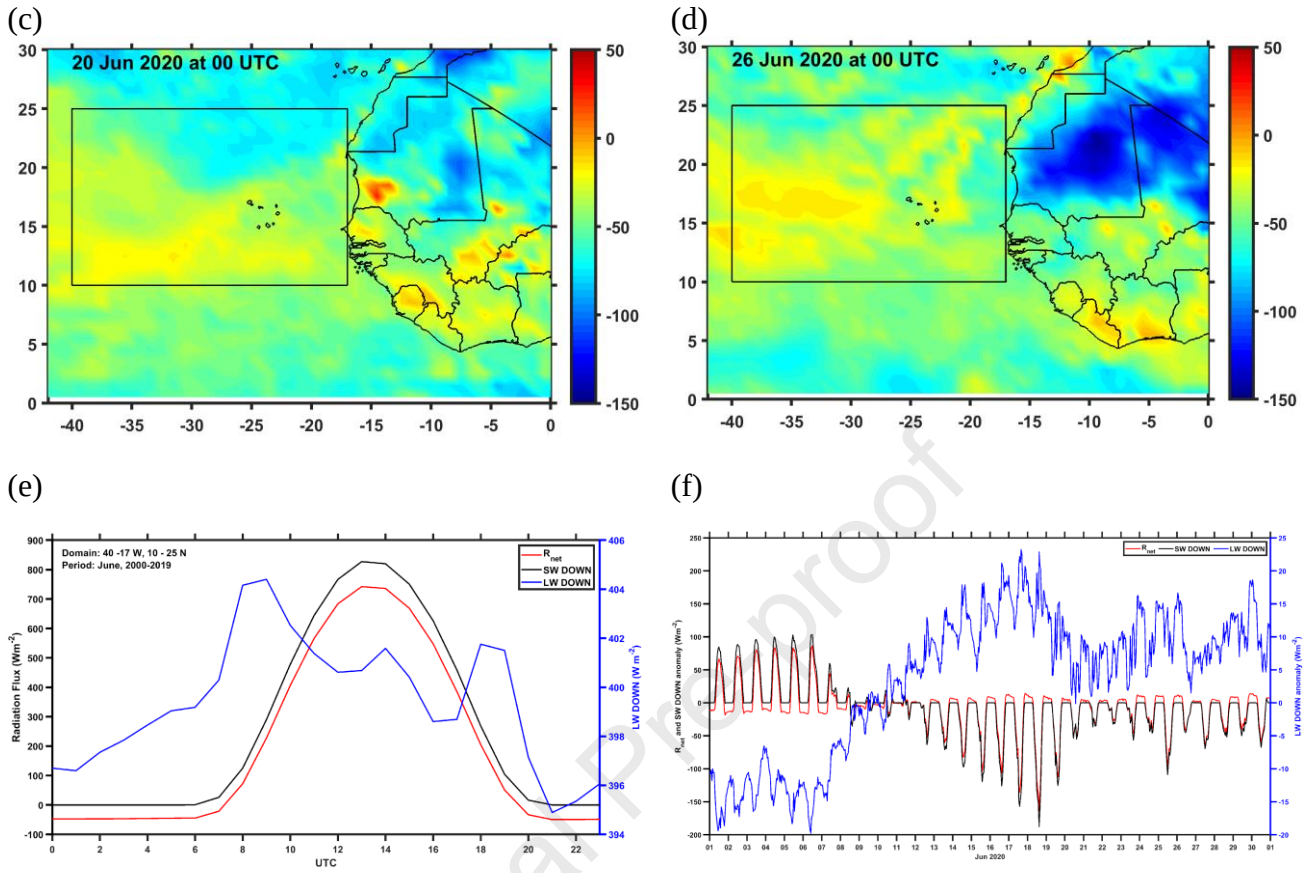
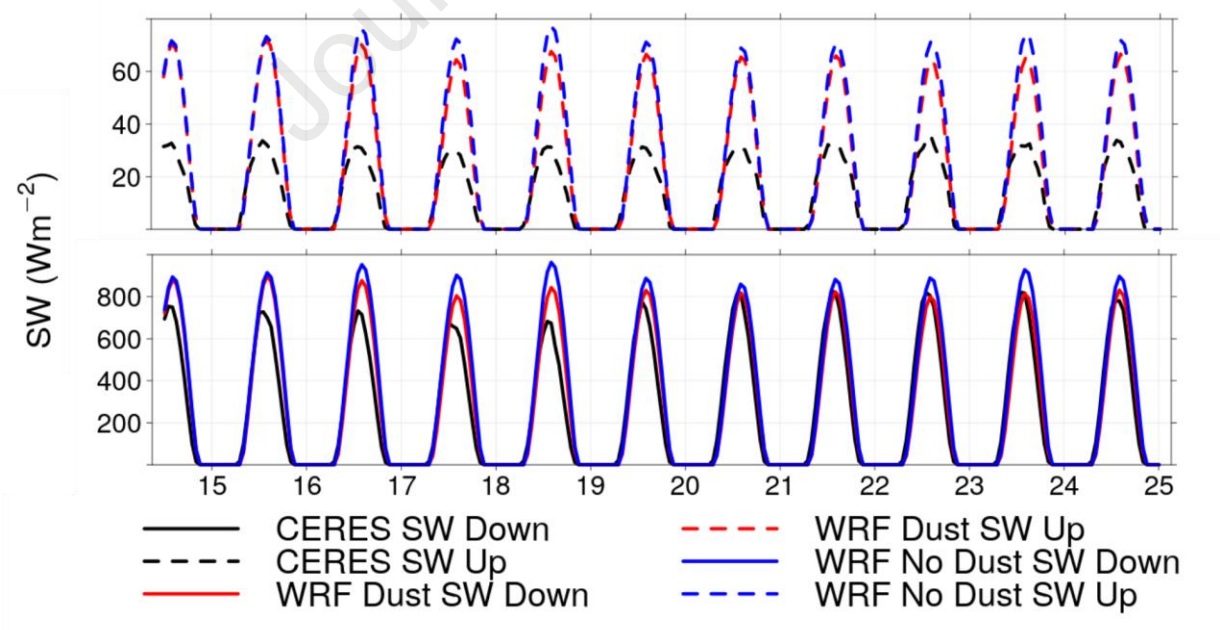


Figure 4. CERES net radiation flux at the surface, R_{net} (W m^{-2}), on 18 June 2020 at (a) 00 UTC and (b) 12 UTC; at 00 UTC on (c) 20 June 2020 and (d) 26 June 2020. (e) Climatological diurnal variation of area-averaged CERES downward short-wave and long-wave and R_{net} fluxes over the black rectangle in Fig. 1a. (f) is as (e) but showing the hourly anomalies for the month of June 2020.

The DREs are also evident in the spatially-averaged time-series plots given in Figs. 4e-f. The R_{net} in the eastern tropical Atlantic typically varies between -50 W m^{-2} at night and +740 W m^{-2} during the day, largely following the diurnal cycle of the downward SW radiation flux. The daily maximum occurs at 13 UTC, when the 20-year standard deviation is roughly 40 W m^{-2}, while the minimum takes place at 21 UTC, when the standard deviation is about 6 W m^{-2}. However, during the June 2020 Saharan dust storm, R_{net} dropped by as much as 166 W m^{-2} during the day (~25% of the mean value), with an anomaly of up to +14 W m^{-2} at night (~28% of the mean value). These numbers are roughly two to four standard deviations away from the mean, which underscores the extreme nature of this event. The nighttime increase in the downward LW radiation flux is also highly anomalous: the largest value of ~23 W m^{-2} is about three standard deviations away from the mean. The reduction in the SW (up to ~190 W m^{-2}) and increase in the LW fluxes are up to three times larger than that modelled by Myhre et al. (2003) in the September 2000 Saharan dust storm, respectively. The former is also twice as large as that reported by Kaskaoutis et al. (2019) for a major dust storm in Greece, when the AOD exceeded 4.

The DRE from WRF can be estimated from the simulations with and without dust, given by the red and blue curves in Fig. 5, respectively. The maximum reduction in downward SW is ~100 W m^{-2} while the increase in downward LW reaches up to +20 W m^{-2}. These magnitudes are comparable to those modelled by Saidou Chaibou et al. (2020) over West Africa, by Haywood et al. (2003) and Highwood et al. (2003) off the coast of Africa, and are in line with those estimated by Anton et al. (2014), who studied a dust storm that affected southeastern Spain, for the predicted range of AODs. The modelled DREs for this event are larger than those estimated by Gutleben et al. (2020) for a dust event in the Caribbean, but smaller than those computed for the extreme September 2015 dust event over the eastern Mediterranean and the Middle East (Uzan et al., 2018), and for a major dust storm in Greece in March 2018 by Kaskaoutis et al. (2019). It is interesting to note that in the run without the dust feedback, the downward SW shows a day-to-day variability that has a comparable magnitude to the DRE, with a decrease of up to ~100 W m^{-2} from 16-17 and 18-19 June, and an increase from 17 to 18 June due to the presence of clouds in the target region. A comparison with the CERES fluxes shows that WRF has a considerable bias: the model overestimates the downward SW by as much as 200 W m^{-2}, while the downward and upward LW fluxes are up to 20 W m^{-2} and 10 W m^{-2} smaller in WRF, respectively. When comparing the WRF simulation without dust and CERES (Figs. 4e-f and 5), the ~200 W m^{-2} difference in downward SW and ~40 W m^{-2} in downward LW are indicative of the net effect of dust, and are in line with the values obtained from the climatology analysis (Fig. 4f).

(a)



(b)

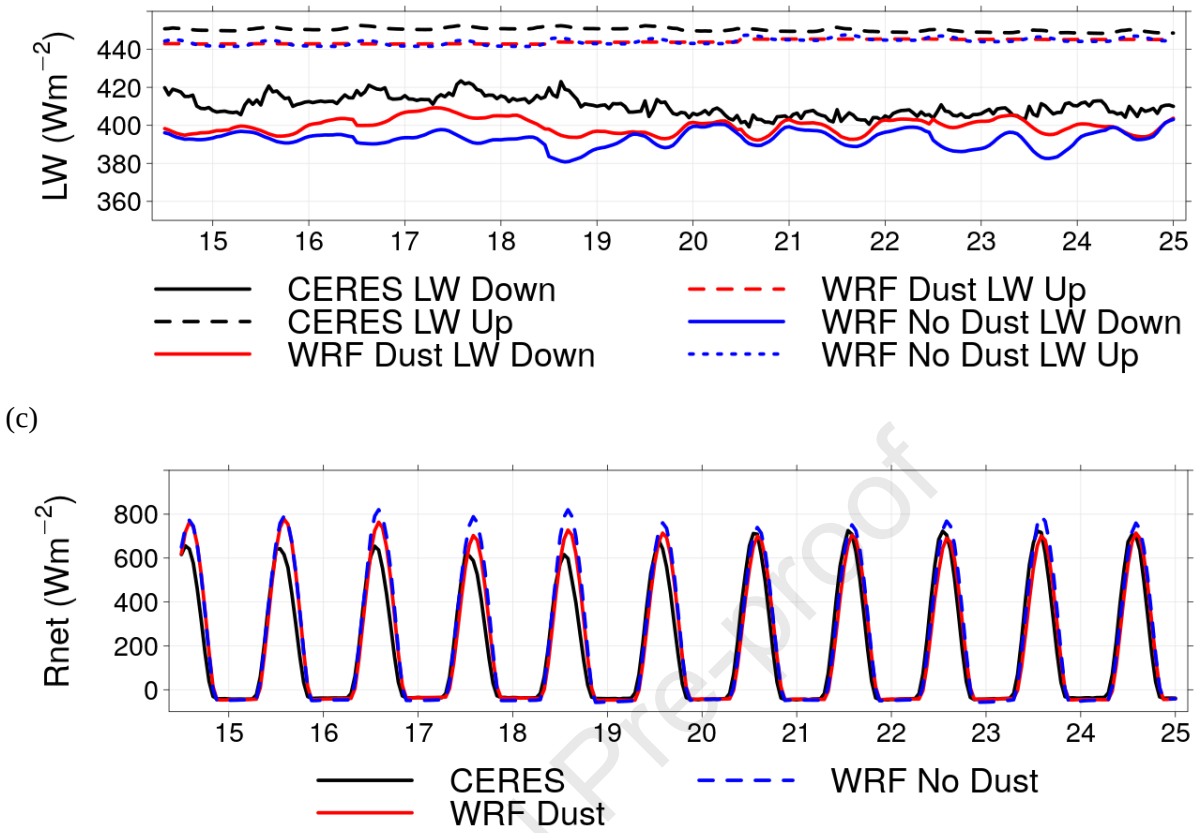


Figure 5. Time series of the upward (dashed line) and downward (solid line) (a) shortwave and (b) longwave radiative fluxes, and (c) net radiative flux (R_{net}; W m^{-2}) from WRF (red) and CERES (black) averaged over 38ºW-17ºW & 10ºN-25ºN and for the period 14-24 June 2020. The predictions of the WRF simulations in which the DRE is accounted for are given by red lines, and those of the run without DRE are plotted in blue lines.

It is interesting to note that the dust effects on the upward SW radiation flux are much smaller than those on the downward SW radiation flux, mostly below 70 W m^{-2}. This can be attributed to the low albedo of the sea surface (~0.06; e.g., Payne, 1972), which absorbs the vast majority of the incoming SW radiation. Similarly, the ~20 W m^{-2} increase in the downward LW radiation flux is in contrast with a <5 W m^{-2} increase in the upward LW radiation flux. The latter is essentially controlled by the surface temperature, which exhibits a reduced variability over water as opposed to land regions due to its higher thermal inertia (e.g., Kawai and Wada, 2007).

The radiative impact of dust on the sea surface and air temperature can be seen in Fig. 6, with Fig. 6a giving the satellite-derived SSTs and Fig. 6b the air temperature from ERA-5. The SSTs, averaged over the eastern tropical Atlantic Ocean, increased by roughly 0.6-1.1 K during the event, a magnitude up to two times that of the climatological standard deviation. The air temperature rose by over 1.8 K, or about three times the climatological standard deviation. While the amplitude of the SST change is comparable to that reported by other studies over the eastern tropical Atlantic during Sahara dust outbreaks (e.g., Martinez Avellaneda et al., 2010; Jordan et al., 2018), the sign

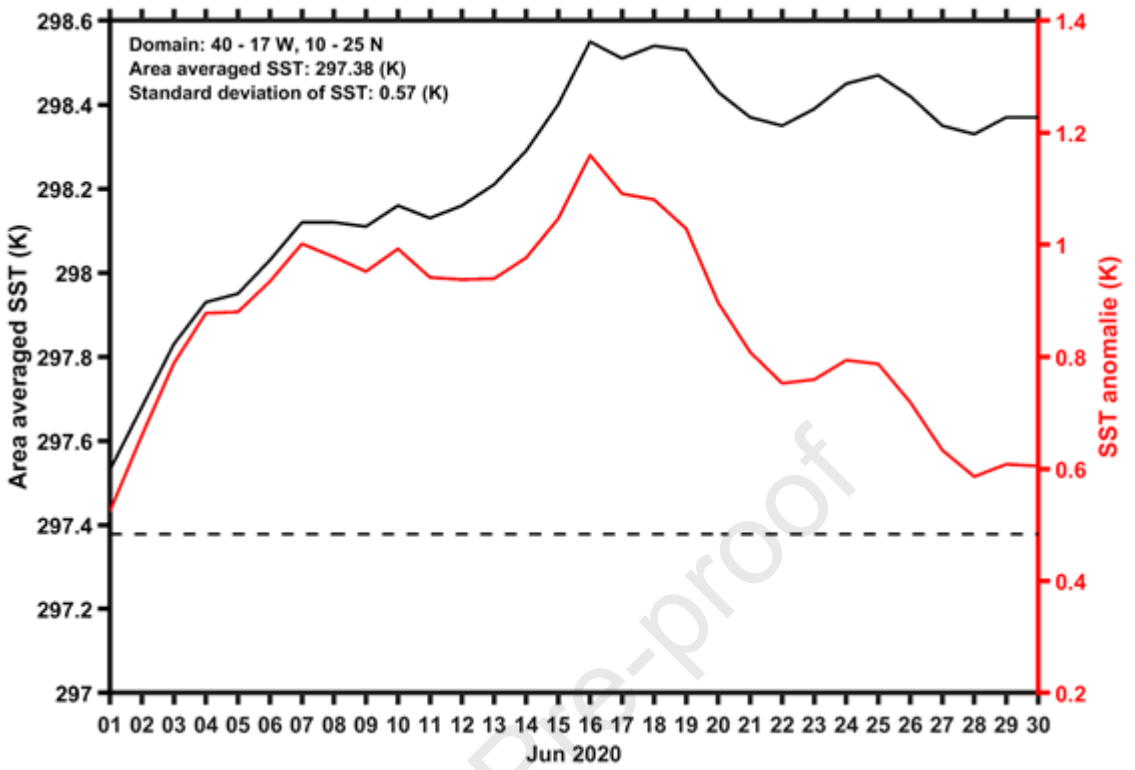
is the opposite. The SST warming is likely due to the extremely high AODs observed in June 2020, for which the heating of the ocean surface by the increased downward LW throughout the day outweighs the cooling due to the reduced downward SW. In fact, the peak in SST anomalies on 24-25 June (Fig. 6a) takes place just after the AOD peak on 23 June (Fig. 2a). The warming of the SSTs is consistent with the R_{net} and total energy flux F_{net} (given by R_{net} plus the heat fluxes) time-series given in Figs. 6c and d, respectively. F_{net} remains relatively high from 15 to 18 June, with anomalies as large as one third of its climatological standard deviation (Fig. 6d). This is an indication of the heating of the surface. In fact, the maximum in SST (Fig. 6a) and 2-meter temperature (Fig. 6b) occurs when the total energy flux at the surface is positive.

The dust aerosols' induced warming over the ocean is contradicting with the findings of previous studies on the dust radiative impact. These studies were mainly based on modelling techniques and concluded that the dust direct effect can increase the surface temperature over higher albedo surface and decrease the surface temperature over lower albedo areas (Xie et al., 2018; Miller 2012; Takemura et al., 2009). However, when considering the dust radiative impact in the longwave and by looking at daytime and nighttime observations separately (daily averaging leads to the cancellation of daytime and nighttime effects), the results are different as evidenced in the current study. Additionally, most of the current atmospheric models miss most of the large dust particles in their simulated atmospheres and tend to deposit these particles too quickly near dust source regions (Adebiyi and Kok, 2020) which leads to an underestimation of the dust radiative impact in the longwave and hence in the net effect. Our results resonate with the findings of a new study (Xian et al., 2020) in which the authors revisited the relationship between tropical cyclones and dust aerosols and found a weak correlation between high dust aerosols and low tropical cyclones activity over the tropical Atlantic Ocean. Should the nighttime/daytime dust effects have been considered separately, the results by Xian et al., (2020) may have been further showing the warming effect of dust aerosols at the surface.

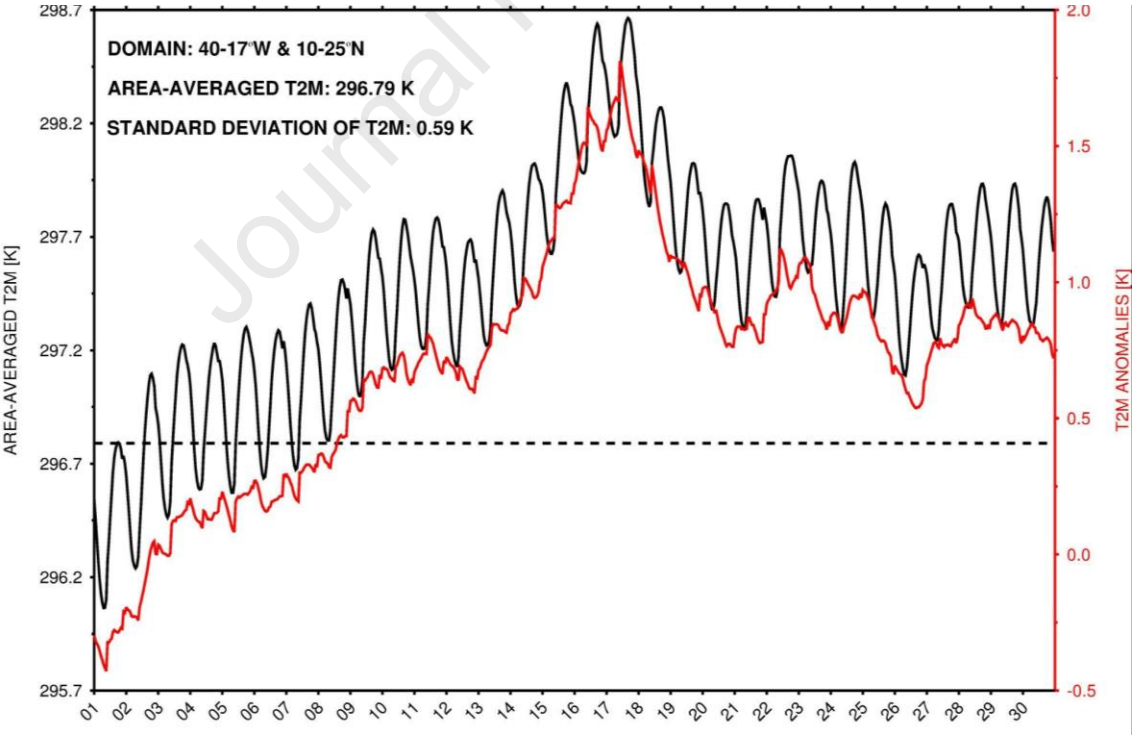
The fact that an extremely dusty environment may lead to higher SSTs can be seen in Fig. 7, which shows SEVIRI RGB and satellite-derived SST anomaly maps on 15, 18 and 23 June 2021. In these figures, dustier regions are co-located with areas of positive SST anomalies exhibiting above-average SSTs in places in excess of 4 K. It is important to note, when analyzing these results, that due to the higher thermal inertia of water, it takes some time for the SSTs to respond to the atmospheric forcing. Finally, it is interesting to note that the R_{net} anomalies from ERA-5, Fig. 6c, are substantially different from those of CERES, Fig. 4f, in particular between 12 and 20 June. This is an indication that the biases in the reanalysis dataset can still be considerable, despite the extensive data assimilation employed.

Journal Pre-proof

(a)

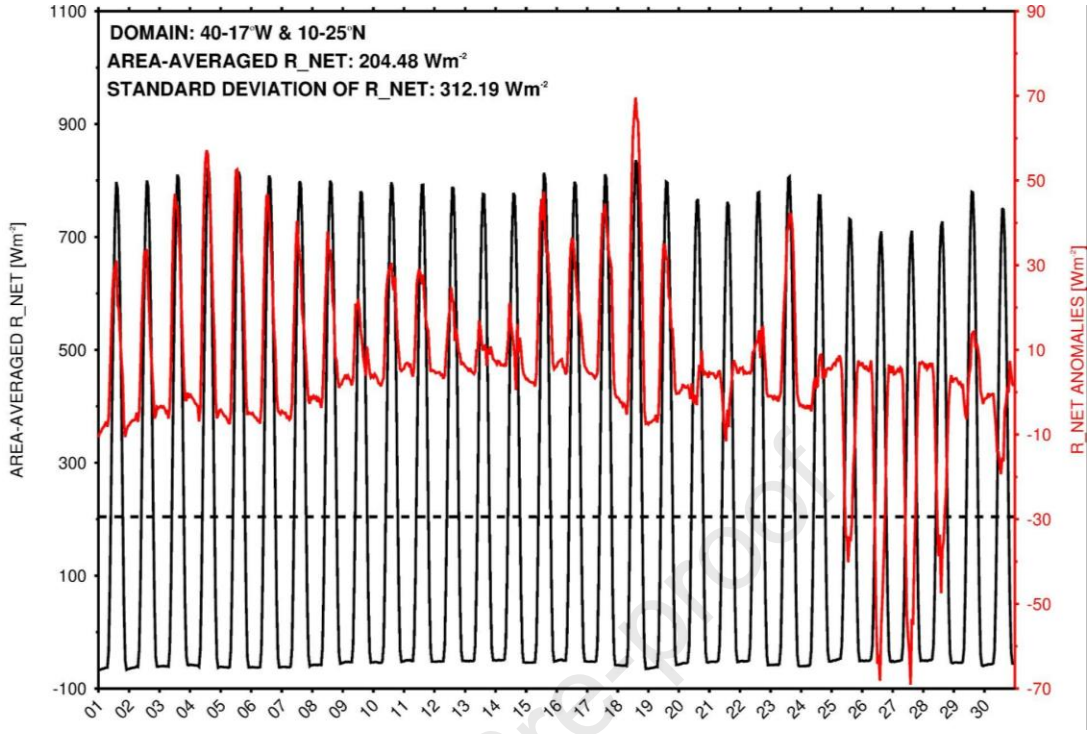


(b)

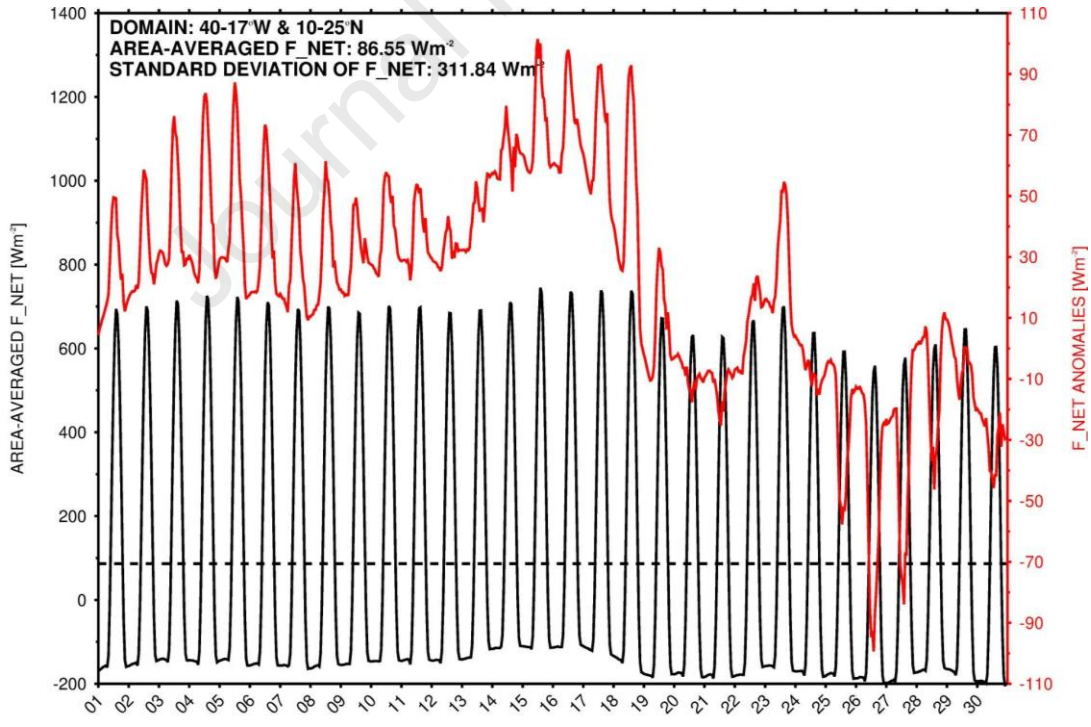


(c)

Journal Pre-proof

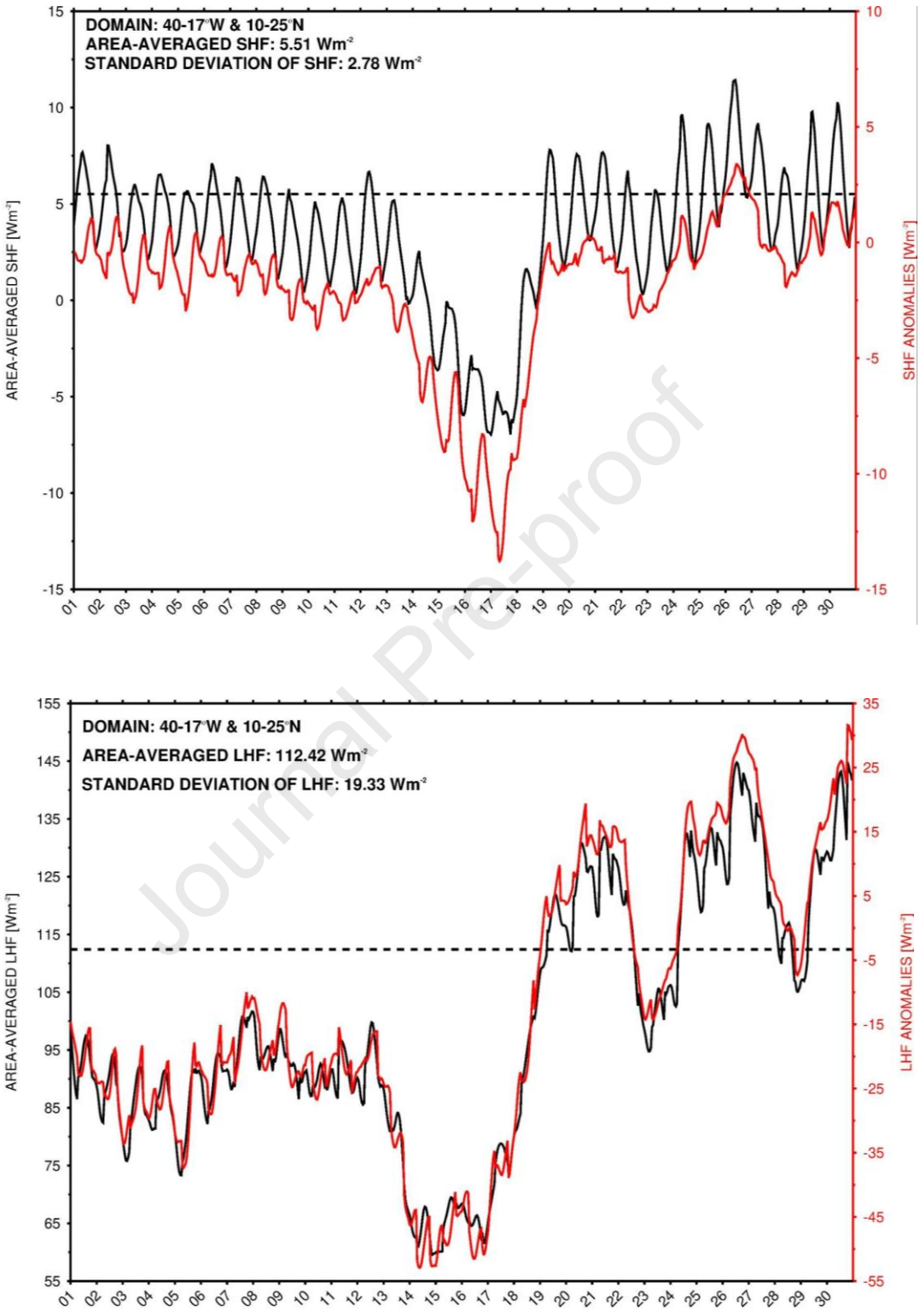


(d)



(e)

Journal Pre-proof

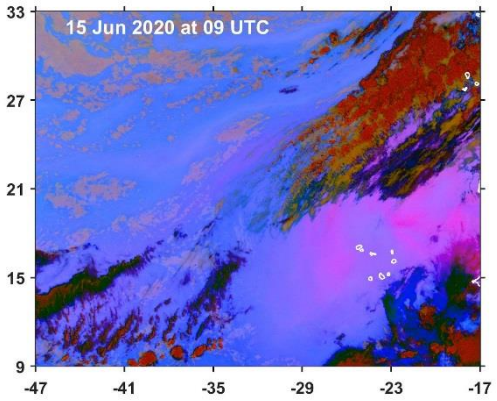


(f)

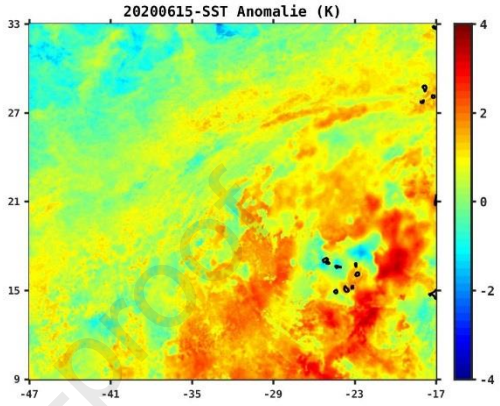
Figure 6. Averaged over 40-17ºW & 10-25ºN (black rectangle in Fig. 1) for the June 2020 actual values and anomalies of (a) Daily SSTs (K) from GHRSST, and ERA-5 (b) 2-meter temperature (K), (c) total radiation flux (R_{net}), (d) total energy flux (F_{net}) at the surface in W m^{-2} (both positive if downward into

the surface), (e) sensible heat flux (SHF) and (f) latent heat flux (LHF) in W m^{-2} (both positive if upwards into the atmosphere). The GHRSST anomalies are computed with respect to the 2002-2019 climatology, while those of ERA-5 are with respect to the 2000-2019 climatology, as GHRSST data is not available prior to 2002. In all panels, the climatological mean and standard deviation are given at the top left, with the former also plotted as a dashed line.

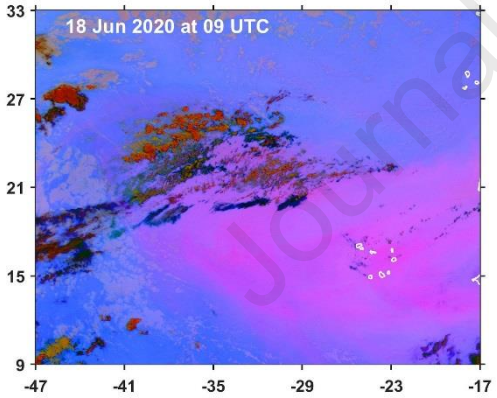
(a)



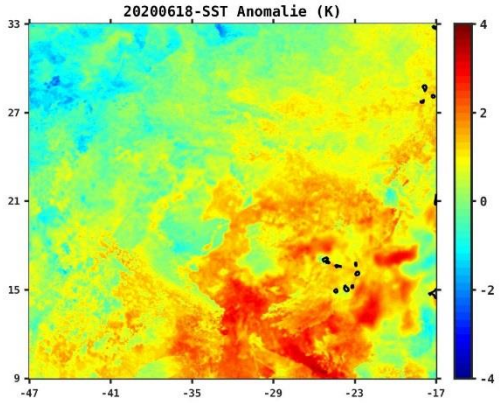
(b)



(c)



(d)



(e)

(f)

Journal Pre-proof

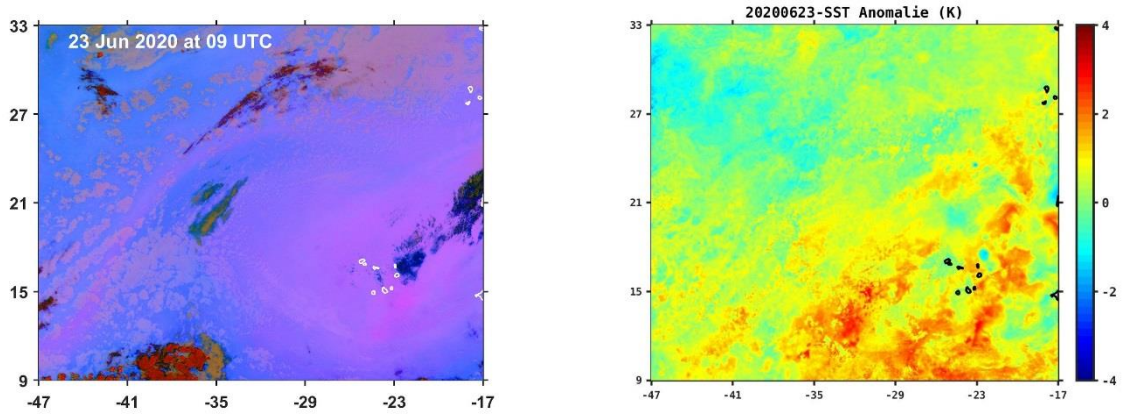


Figure 7: SEVIRI dust RGB snapshot at 09 UTC on (a) 15 June, (c) 18 June and (e) 23 June 2021. Thick high-level clouds are shaded in orange or brown; thin high-level clouds appear very dark (nearly black); dust is given in magenta or pink; sandy regions are highlighted in white; dry land is shaded in pale green. (b), (d) and (f) are GHRSST anomalies with respect to the 2002-2019 climatology on the same days. All fields are shown for the domain 47ºW-17ºW and 9ºN-33ºN.

As far as the heat fluxes are concerned (Figs. 6e and 6f), the SHF and LHF drop by up to 14 and 54 $W\,m^{-2}$, respectively, higher than the respective standard deviations. The variations of the SHF and LHF estimated for this event are roughly one half and four times larger than those modelled by Saidou Chaibou et al. (2020) over West Africa, respectively. The larger magnitude-change in the LHF compared to the SHF is in line with the fact that the target region in Saidou Chaibou et al. (2020) is over the desert, whereas here the fluxes are averaged over the ocean. The negative SHF is consistent with a warmer air temperature compared to the SSTs (i.e. downward pointing fluxes). Once the atmosphere becomes clearer, the surface-to-air temperature gradient decreases (Figs. 6a-b), which leads to a decrease in the SHF (i.e. it is less negative) and an increase in the LHF (enhanced surface evaporation). The warming of the surface seen here has important implications for the genesis and intensification of tropical storms: while the presence of a drier and dustier environment inhibits the formation of tropical disturbances (e.g., Reed et al., 2019), warmer SSTs and the resultant warming and moistening of the boundary layer have the opposite effect (e.g., Emanuel, 2005). As the dust plume extended all over the Atlantic Ocean (Fig. 3d and 3f), mostly near its primary breeding region just off the coast of Africa (Haggard et al., 1958), it is possible that the unprecedented June 2020 Saharan dust storm played a role in what was the most active Atlantic hurricane season on record, in particular in its early and rapid onset (Blackwell, 2020).

4. Conclusions

In this study, the dust loading and radiative forcing for the June 2020 Saharan dust storm are estimated using a combination of observational and modelling products.

On 18 June, during the peak of the event, AOD estimates from satellite reached ~5, with the MERRA-2 reanalysis and WRF underestimating it by up to one index unit. The dust loading over the eastern tropical Atlantic is estimated at 7.9 Tg, a similar magnitude to that calculated over land during previous major dust storms in the Sahara Desert (Bou Karam et al. 2009, 2010, 2014). A comparable dust loading was observed in the following days, underscoring the persistent nature of the emissions during this event.

The spatially-averaged reduction over the eastern tropical Atlantic Ocean in the downward SW radiation flux reached ~190 $W m^{-2}$ on 18 June, with an increase in the downward LW radiation by up to 23 $W m^{-2}$, both larger than those observed at a single station in other major dust storms (e.g., Myhre et al., 2003; Kaskaoutis et al., 2019). As opposed to other events, however, there was an increase in SSTs by as much as +1.1 K, and in the air temperature by up +1.8 K. This arises due to a net warming of the surface, with an anomaly in the total energy flux of up to ~100 $W m^{-2}$, roughly a third of its climatological standard deviation. A comparison of the dust plume with the SSTs, both estimated from satellite data, further suggests that heavy dust loadings may lead to higher SSTs.

Over the last few decades, dust outbreaks from the Sahara Desert have been thought to induce a net cooling at the surface and therefore contribute to the decrease in tropical storm activity over the tropical Atlantic (e.g., Evan et al., 2006). However, our results show that the June 2020 historical dust storm induced a net warming over a sustained period of time. This is in line with the findings of recent studies (Xian et al., 2020), which showed that the warming effect of dust aerosols is larger than previously thought (e.g., Adebiyi and Kok, 2020; Francis et al., 2020a).

These findings stress the importance of representing the radiative effects of dust aerosols in general circulation models (GCMs) as well as in weather and climate models, in particular those dedicated to the study and forecast of tropical storms and hurricanes. For example, the 2020 Atlantic hurricane season was record-breaking and was off to a fast start in May-July (Blackwell, 2020). Given that the Saharan dust reached all the way to North America, the aforementioned increase in SSTs may have promoted the more active storm season, in particular as the largest SST increases were around the breeding region for the so-called Cape Verde hurricanes, which are typically the strongest of the season (Haggard, 1958). More investigation is needed in future studies in order to disentangle the complex interconnection between the dust radiative forcing and storm development and intensity. In particular, numerical experiments can be conducted to explore the sensitivity of the SST response to varying levels of dust loading. Previous studies on the dust radiative impact using GCMs have shown that the dust direct effect can increase the surface temperature over higher albedo surface and decrease the surface temperature over lower albedo areas (Xie et al., 2018; Miller 2012; Takemura et al., 2009). The findings of the current study do not support those conclusions and invite the scientific community to investigate more carefully the dust radiative impact in the longwave especially during night, and recommend a better

representation in GCMs of dust aerosols' size distribution (where large size particles are currently underrepresented) and optical properties.

Acknowledgments

We wish to acknowledge the contribution of Khalifa University's high-performance computing and research computing facilities to the results of this research. The SEVIRI satellite images were downloaded from The European Organisation for the Exploitation of Meteorological Satellites website (https://eoportal.eumetsat.int/). On the National Oceanic and Atmospheric Organization's website, VIIRS (https://www.star.nesdis.noaa.gov/smcd/emb/viirs_aerosol/products.php), CERES (https://ceres.larc.nasa.gov/data/) and GHRSST (http://ghrsst.nodc.noaa.gov) data are available, while MODIS (https://modis.gsfc.nasa.gov/data/) and AERONET (https://aeronet.gsfc.nasa.gov/) data can be downloaded on the National Aeronautics and Space Administration's website. All the data used in the present analysis are available here https://zenodo.org/record/4572733#.YKYoQqgzY2x.

Conflict of Interest: The authors declare they don't have any conflict of interest.

Journal Pre-proof

References

Adebiyi A. A., J. F. Kok, (2020), Climate models miss most of the coarse dust in the atmosphere. Science Advances,. 6, eaaz9507, doi: 10.1126/sciadv.aaz9507.

Al-Hemoud, A., Al-Sudairawi, M., Neelamanai, S., Naseeb, A. and Behbehani, W. (2017), Socioeconomic effect of dust storms in Kuwait. Arabic Journal of Geosciences, 10(18), 1-9, doi: 10.1007/s12517-016-2816.

Alpert, P. and Ganor, E. (1998), Sahara mineral dust measurements from TOMS: comparison to surface observations over the Middle East for the extreme dust storm, March 14-17, 1998. Journal of Geophysical Research, 106, 18275-18286, doi: 10.1029/2000JD900366.

Anton, M., Valenzuela, A., Mateos, D., Alados, I., Foyo-Moreno, I., Olmo, F. J. and Alados-Arboledas, L. (2014), Longwave aerosol radiative effects during an extreme desert dust event in southeastern Spain. Atmospheric Research, 149, 18-23, doi: 10.1016/j.atmosres.2014.05.022.

Azua-Bustos, A., Gonzalez-Silva, C., Fernandez-Martinez, M. A., Arenas-Fajardo, C., Fonseca, R., Martin-Torres, F. J., Fernandez-Sampedro, M., Fairen, A. G. and Zorzano, M.-P. (2019), Aeolian transport of viable microbial life across the Atacama Desert, Chile: Implications for Mars. Scientific Reports, 9, 11024, doi: 10.1038/s41598-019-47394-z.

Balkanski, Y., Bonnet, R., Boucher, O., Checa-Garcia, R. and Servonnat, J. (2021), Dust Induced Atmospheric Absorption Improves Tropical Precipitations in Climate Models. Atmospheric Chemistry and Physics Discussion, Under Review, doi: 10.5194/acp-2021-12.

Barnard, J. C., Fast, J. D., Paredes-Miranda, G., Arnott, W. P. and Laskin, A. (2010), Technical Note: Evaluation of the WRF-Chem Aerosol Chemical to Aerosol Optical Properties Module using data from the MILAGRO campaign. Atmospheric Chemistry and Physics, 10, 7325-7340, doi: 10.5194/acp-10-7325-2010.

Bellouin, N., Quaas, J., Gryspeerdt, E., Kinne, S., Stier, P., Watson-Parris, D., Boucher, O., Carslaw, K. S., Christensen, M., Daniau, A.-L., Dufresne, J.-L., Feingold, G., Fiedler, S., Forster, P., Gettelman, A., Haywood, J. M., Lohmann, U., Malavelle, F., Mauritsen, T., McCoy, D. T., Myhre, G., Mulmenstadt, J., Neubauer, D., Possner, A., Rugenstein, M., Sato, Y., Schulz, M., Schwartz, S. E., Sourdeval, O., Storelvmo, T., Toll, V., Winker, D. and Stevens, B. (2020), Bounding Global Aerosol Radiative Forcing of Climate Change. Reviews of Geophysics, 58, e2019RG000660, doi: 10.1029/2019RG000660.

Blackwell, J. (2020), Record-breaking Atlantic hurricane season draws to an end. National Oceanic and Atmospheric Administration, available online at https://www.noaa.gov/media-release/record-breaking-atlantic-hurricane-season-draws-to-end.

Journal Pre-proof

Bou Karam, D., Flamant, C., Cuesta, J., Pelon, J. and Williams, E. (2010), Dust emission and transport associated with a Sharan depression: February 2007 case. Journal of Geophysical Research, 115, D00H27, doi: 10.1029/2009JD012390.

Bou Karam, D., Flamant, C., Tulet, P., Chaboureau, J.-P., Dabas, A. and Todd, M. C. (2009), Estimate of Sahelian dust emissions in the intertropical discontinuity region of the West African Monsoon. Journal of Geophysical Research, 114, D13106, doi: 10.1029/2008JD011444.

Bou Karam, D., Williams, E., Janiga, M., Flamant, C., McGraw-Herdeg, M., Cuesta, J., Auby, A. and Thorncroft, C. (2014), Synoptic-scale dust emissions over the Sahara Desert initiated by a moist convective cold pool in early August 2006. Quarterly Journal of the Royal Meteorological Society, 140, 2591-2607, doi: 10.1007/qj.2326.

Buchard, V., Randles, C. A., da Silva, A. M., Darmenov, A., Colarco, P. R., Govindaraju, R., Ferrare, R., Hair, J., Beyersdorf, A. J., Ziemba, L. D. and Yu, H. (2017), The MERRA-2 Aerosol Reanalysis, 1980 Onward. Part II: Evaluation and Case Studies. Journal of Climate, 30, 6851-6872, doi: 10.1175/JCLI-D-16-0613.1.

Chen, D., Liu, Z., Davis, C. and Gu, Y. (2017), Dust radiative effects on atmospheric thermodynamics and tropical cyclogenesis over the Atlantic Ocean using WRF-Chem coupled with an AOD data assimilation system. Atmospheric Chemistry and Physics, 17, 7917-7939, doi: 10.5194/acp-17-7917-2017.

Chu, D. A., Kaufman, Y. J., Ichoku, C., Remer, L. A., Tanre, D. and Holben, B. N. (2002), Validation of MODIS aerosol optical depth retrieval over land. Geophysical Research Letters, 29(12), doi: 10.1029/2001GL013205.

Choobari, A., Zawar-Reza, P. and Sturnman, A. (2014), The global distribution of mineral dust and its impacts on the climate system: A review. Atmospheric Research, 138, 152-165, doi: 10.1016/j.atmosres.2013.11.007.

Colarco, P. R., Toon, O. B. and Holben, B. N. (2003), Saharan dust transport to the Caribbean during PRIDE: 1. Influence of dust sources and removal mechanisms on the timing and magnitude of downwind aerosol optical depth events from simulations of in situ and remote sensing observations. Journal of Geophysical Research: Atmospheres, 108, 8589, doi: 10.1029/2002JD002658.

Di Bagio, C., Formenti, P., Balkanski, Y., Caponi, L., Cazaunau, M., Pangui, E., Journet, E., Nowak, S., Caquineau, S., Andrae, O. M., Kandler, K., Saeed, T., Piketh, S., Seibert, D., Williams, E., Doussin, J. F. C. (2017), Global scale variability of the mineral dust long-wave refractive index: A new dataset of in situ measurements for climate modeling and remote sensing. Atmospheric Chemistry and Physics, 17, 1901-1929, doi: 10.5194/acp-17-1901-2017.

Doelling, D. R., Loeb, N. G., Keyes, D. F., Nordeen, M. L., Morstad, D., Nguyen, C., Wielicki, B. A., Young, D. F. and Sun, M. (2013), Geostationary Enhanced Temporal Interpolation for CERES Flux

Journal Pre-proof

Products. Journal of Atmospheric and Oceanic Technology, 30, 1072-1090, doi: 10.1175/JTECH-D-12-00136.1

Doelling, D. R., Sun, Nguyen, L. T., Nordeen, M. L., Haney, C. O., Keyes, D. F. and Mlynczak, P. E. (2016), Advances in Geostationary-Derived Longwave Fluxes for the CERES Synoptic (SYN1deg) Product. Journal of Atmospheric and Oceanic Technology, 33, 503-521, doi: 10.1175/JTECH-D-15-0147.1.

Dubovik O., A. Sinyuk, T. Lapyonok, B.N. Holben, M. Mishchenko, P. Yang, T.F. Eck, H. Volten, O. Muñoz, B. Veihelmann, W.J. van der Zande, J.-F. Leon, M. Sorokin, I. Slutsker, Application of spheroid models to account for aerosol particle non sphericity in remote sensing of desert dust J. Geophys. Res., 111 (2006), p. D11208, 10.1029/2005JD006619

Dy, C. Y. and Fung, J. C. H. (2016), Updated global soil map for the Weather Research and Forecasting model and soil moisture initialization for the Noah land surface model. Journal of Geophysical Research, 121, 8777-8800, doi: 10.1002/2015JD024558.

Eltahan, M., Shokr, M. and Sherif, A. O. (2018), Simulation of Severe Dust Events over Egypt Using Tuned Dust Schemes in Weather Research Forecast (WRF-Chem). Atmosphere, 9, 246, doi: 10.3390/atmos9070246.

Emanuel, K. (2005), Increasing destructiveness of tropical cyclones over the past 30 years. Nature, 436, 686-688, doi: 10.1038/nature03906.

Evan, A. T., Dunion, J., Foley, J. A., Heidinger, A. K., and Velden, C. S. (2006), New evidence for a relationship between Atlantic tropical cyclone activity and African dust outbreaks, Geophys. Res. Lett., 33, L19813, doi:10.1029/2006GL026408.

Evan, A. T., Foltz, G. R. and Zhang, D. (2012), Physical Response of the Tropical-Subtropical North Atlantic Ocean to Decadal-Multidecadal Forcing by African Dust. Journal of Climate, 25, 5817-5829, doi: 10.1175/JCLI-D-11-00438.1.

Evan, A. T., Foltz, G. R., Zhang, D. and Vimont, D. J. (2011), Influence of African dust on ocean-atmosphere variability in the tropical Atlantic. Nature Geosciences, 4, 762-765, doi: 10.1038/ngeo1276.

Flaounas, E., Kotroni, V., Lagouvardos, K., Klose, M., Flamant, C. and Giannaros, T. M. (2017), Sensitivity of the WRF-Chem (V3.6.1) model to different dust emission parametrisation: assessment in the broader Mediterranean region. Geoscientific Model Development, 10, 2925-2945, doi: 10.5194/gmd-10-2925-2017.

Francis, D., Alshamsi, N., Cuesta, J., Isik, A. G. and Dundar, C. (2019), Cyclogenesis and Density Currents in the Middle East and the Associated Dust Activity in September 2015. Geosciences, 9(9), 376, doi: 10.3390/geosciences9090376.

Journal Pre-proof

Francis, D. Chaboureau, J.-P., Nelli, N., Cuesta, J., Al Shamsi, N., Temimi, M., Pauluis, O. and Xue, L. (2020a), Summertime dust storms over the Arabian Peninsula and impacts on radiation, circulation, cloud development and rain. Atmospheric Research, 250, 105364, doi: 10.1016/j.atmosres.2020.105364.

Francis, D., Fonseca, R., Nelli, N., Cuesta, J., Weston, M., Evan, A. and Temimi, M. (2020b), The atmospheric drivers of the major Saharan dust storm in June 2020. Geophysical Research Letters, 47, e2020GL090102, doi: 10.1029/2020GL090102.

Gelato, R., McCarty, W., Suarez, M. J., Todling, R., Molod, A., Takacs, L., Randles, C. A., Darmenov, A., Bosilovich, M. G., Reichle, R., Wargan, K., Coy, L., Cullather, R., Draper, C., Akella, S., Buchard, V., Conaty, A., da Silva, A. M., Gu, W., Kim, G.-K., Koster, R., Lucchesi, R., Merkova, D., Nielsen, J. E., Partyka, G., Pawson, S., Putman, W., Rienecker, M., Schubert, S. D., Sienkiewicz, M. and Zhao, B. (2017), The Modern-Era Retrospective Analysis for Research and Applications, version 2 (MERRA-2). Journal of Climate, 30, 5419-5454, doi: 10.1175/JCLI-D-16-0758.1.

Ginnadaki, D., Pizzer, A. and Lelieveld, J. (2014), Modeled global effects of airborne desert dust on air quality and premature mortality. Atmospheric Chemistry and Physics, 14, 957-968, doi: 10.5194/acp-14-957-2014.

Ginoux, P., Chin, M., Tegen, I., Goddard, T. and In, G. (2001), Sources and distributions of dust aerosols simulated with the GOCART model. Journal of Geophysical Research: Atmospheres, 106, 20255-20273, doi: 10.1029/2000JD000053.

Grell, G. A. and Dvnyi, D. (2002), A generalized approach to parameterizing convection combining ensemble and data assimilation techniques. Geophysical Research Letters, 29, 10-13, doi: 10.1029/2002GL015311.

Grell, G. A., Peckham, S. E., Schmitz, R., McKeen, S. A., Frost, G., Skamarock, W. C. and Eder, B. (2005), Fully coupled "online" chemistry with the WRF model. Atmospheric Environment, 39, 6957-6975, doi: 10.1016/j.atmosenv.2005.04.027.

Griffin, D. W., Kellogg, C. A., Garrison, V. H and Shinn, E. A. (2002), The Global Transport of Dust: An Intercontinental river of dust, microorganisms and toxic chemical flows through the Earth's atmosphere. American Scientist, 90(3), 228-235, doi: 10.1511/2002.3.228.

Gutleben, M., Grob, S., Wirth, M. and Mayer, B. (2020), Radiative effects of long-range-transported Saharan air layers as determined from airborne lidar measurements. Atmospheric Chemistry and Physics, 20, 12313-12327, doi: 10.5194/acp-20-12313-2020.

Haggard, W. H. (1958), The Birthplace of North Atlantic Tropical Storms. Monthly Weather Review, 86(10), 397-404, doi: 10.1175/1520-0493(1958)086<0397:TBONAT>2.0.CO;2.

Journal Pre-proof

Hamzeh, N. H., Karami, S., Kaskaoutis, D. G., Tegen, I., Moradi, M. and Opp, C. (2021), Atmospheric Dynamics and Numerical Simulations of Six Frontal Dust Storms in the Middle East Region. Atmosphere, 12, 125, doi: 10.3390/atmos12010125.

Haywood, J. and Boucher, O. (2000), Estimates of the direct and indirect radiative forcing due to tropospheric aerosols: A review. Reviews of Geophysics, 38(4), 513–543, doi: 10.1029/1999RG000078.

Haywood J.M., R.P. Allan, I. Culverwell, T. Slingo, S. Milton, J. Edwards, N. Clerbaux
Can desert dust explain the outgoing longwave radiation anomaly over the Sahara during July 2003? J. Geophys. Res., 110 (2005), p. D05105, 10.1029/2004JD005232

Haywood, J. M., Francis, P., Osborne, S. R., Glew, M., Loeb, N., Highwood, E., Tanre, D., Myhre, G., Formenti, P. and Hirst, E. (2003), Radiative properties and direct radiative effect of Saharan dust measured by the C-130 aircraft during SHADE: 1. Solar spectrum. Journal of Geophysical Research, 108(D18), 8577, 10.1029/2002JD002687.

Heald C.L., D.A. Ridley, J.H. Kroll, S.R.H. Barrett, K.E. Cady-Pereira, M.J. Alvarado, C.D. Holmes, Contrasting the direct radiative effect and direct radiative forcing of aerosols, Atmos. Chem. Phys., 14 (2014), pp. 5513-5527, 10.5194/acp-14-5513-2014.

Heinold B., I. Tegen, K. Schepanski, O. Hellmuth, Dust Radiative Feedback on Saharan Boundary Layer Dynamics and Dust Mobilization Geophys. Res. Lett., 35 (2008), p. L20817, 10.1029/2008GL035319.

Hersbach, H., Bell, B., Berrisford, P., Dahlgren, P., Horanyi, A., Munoz-Sebater, J., Nicolas, J., Radu, R., Schepers, D., Simmons, A., Soci, C. (2020), The ERA5 Global Reanalysis: achieving a detailed record of the climate and weather for the past 70 years. European Geophysical Union General Assembly 2020, May 3 - 8, Vienna, Austria, doi: 10.5194/egusphere-egu2020-10375.

Highwood, E. J., Haywood, J. M., Silverstone, M. D., Newman, S. M. and Taylor, J. P. (2003), Radiative properties and direct effect of Saharan dust measured by the C-130 aircraft during SHADE. 2: Terrestrial spectrum. Journal of Geophysical Research, 108(D18), 8578, 10.1029/2002JD002552.

Holben, B. N., Eck, T. F., Slutsker, I., Tanre, D., Buis, J. P., Setzer, A., Vermote, E., Reagan, J. A., Kaufman, Y. J., Nakajima, T., Lavenu, F., Jankowiak, I. and Smirnov, A. (1998), AERONET - A Federated Instrument Network and Data Archive for Aerosol Characterization. Remote Sensing of the Environment, 66, 1-16, doi: 10.1016/s0034-4257(98)00031-5.

Hong, S. Y., Noh, Y. and Dudhia, J. (2006), A new vertical diffusion package with an explicit treatment of entrainment processes. Monthly Weather Review, 134, 2318-2341, doi: 10.1175/MWR3199.1.

Iacono, M. J., Delamere, J. S., Mlawer, E. J., Shepherd, M. W., Clough, S. A. and Collins, W. D. (2008), Radiative forcing by long-lived greenhouse gases: Calculations with the AER radiative transfer models. Journal of Geophysical Research, 113, D13103, doi: 10.1029/2008JD009944.

Ito, A., Abediyi, A. A., Huang, Y. and Kok, J. F. (2021), Less atmospheric radiative heating due to aspherical dust with coarser size. Atmospheric Chemistry and Physics Discussion (Under Review), doi: 10.5194/acp-2021-134.

Jia R., Y. Liu, S. Hua, Q. Zhu, T. Shao, Estimation of the aerosol radiative effect over the Tibetan Plateau based on the latest CALIPSO product, J. Meteorol. Res., 32 (2018), pp. 707-722, 10.1007/s13351-018-8060-3.

Jimenez, P. A., Dudhia, J., Gonzlez-Rouco, J. F., Navarro, J., Montvez, J. P. and Garcia-Bustamante, E. (2012), A revised scheme for the WRF surface layer formulation. Monthly Weather Review, 140, 898-918, doi: 10.1175/MWR-D-11-00056.1.

Jordan, A. K., Gnanadesikan, A. and Zaitchik, B., (2018), Simulated Dust Aerosol Impacts on Western Sahelian Rainfall: Importance of Ocean Coupling. Journal of Climate, 31(22), 9107-9124, doi: 10.1175/JCLI-D-17-0819.1.

Kabatas, B., Pierce, R. B., Unal, A., Rogal, M. J. and Lenzen, A. (2018), April 2008 Saharan dust event: Its contribution to PM10 concentrations over the Anatolian Peninsula and relation with synoptic conditions. Science of The Total Environment, 533, 317-328, doi: 10.1016/j.scitotenv.2018.03.150.

Kaskaoutis, D. G., Dumka, U. C., Rashki, A., Psiloglou, B. E., Gavriil, A., Mofidi, A., Petrinoli, K., Karagiannis, D. and Kambezidis, H. D. (2019), Analysis of intense dust storms over the eastern Mediterranean in March 2018: Impact on radiative forcing and Athens air quality. Atmospheric Environment, 209, 23-39, doi: 10.1016/j.atmosenv.2019.04.025.

Kaufman, Y. J., Tanre, D., Rmer, L. A., Vermote, E. F., Chu, A. and Holben, B. N. (1997), Operational remote sensing of tropospheric aerosol over land from EOS moderate resolution imaging spectroradiometer. Journal of Geophysical Research, 102, 17501-17067, doi: 10.1029/96JD03988.

Kawai, Y. and Wada, A. (2007), Diurnal sea surface temperature variation and its impact on the atmosphere and ocean: A review. Journal of Oceanography, 63, 721-744, doi: 10.1007/s10872-007-0063-0.

Kok, J. F., Adebiyi, A. A., Albani, S., Balkanski, Y., Checa-Garcia, R., Chin, M., Colarco, P. R., Hamilton, D. S., Huang, Y., Ito, A., Klose, M., Li, L., Mahowald, N. M., Miller, R. L., Obiso, V., Pérez García-Pando, C., Rocha-Lima, A., and Wan, J. S.: Contribution of the world's main dust source regions to the global cycle of desert dust, Atmos. Chem. Phys., 21, 8169–8193, https://doi.org/10.5194/acp-21-8169-2021, 2021.

Kosmopoulos P.G., S. Kazadzis, M. Taylor, E. Athanasopoulou, O. Speyer, P.I. Raptis, E. Marinou, E. Proestakis, S. Solomos, E. Gerasopoulos, V. Amiridis, A. Bais, C. Kontoes, Dust impact on surface solar irradiance assessed with model simulations, satellite observations and ground-based measurements, Atmos. Meas. Tech., 10 (2017), pp. 2435-2453, 10.5194/amt10-2435-2017

Legrand, S. L., Polashenski, C., Letcher, T. W., Creighton, G. A., Peckham, E. and Cetola, J. D. (2018), The AFWA Dust Emissions Scheme for the GOCART Aerosol Model in WRF-Chem. Geoscientific Model Development, 12, 131-166, doi: 10.5194/gmd-12-131-2019.

Levy, R. and Hsu, C. (2015a), MODIS Atmosphere L2 Aerosol Product. NASA MODIS Adaptive Processing System, Goddard Space Flight Center, USA, doi: 10.5067/MODIS/MOD04_L2.061.

Levy, R. and Hsu, C. (2015b), MODIS Atmosphere L2 Aerosol Product. NASA MODIS Adaptive Processing System, Goddard Space Flight Center, USA, doi: 10.5067/MODIS/MYD04_L2.061.

Levy, R. C., Remer, L. A., Martins, J. V., Kaufman, Y. J., Plana-Fattori, A., Redemann, J. and Wenny, B. (2005), Evaluation of the MODIS Aerosol Retrievals over Ocean and Land during CLAMS. Journal of Atmospheric Sciences, 62(4), 974-992, doi: 10.1175/JAS3391.1.

Lin, Y. L., Farley, R. D. and Orville, H. D. (1983), Bulk parameterization of the snow field in a cloud model. Journal of Applied Meteorology and Climatology, 22, 1065-1092, doi: 10.1175/1520-0450(1983)022<1065:BPOTSF>2.0.CO;2.

Liu, L., Huang, X., Ding, A. and Fu, C. (2016), Dust-induced radiative feedbacks in north China: A dust storm episode modeling study using WRF-Chem. Atmospheric Environment, 129, 43-54, doi: 10.1016/j.atmosenv.2016.01.019.

Loveland, T. R., Reed, B. C., Ohlen, D. O., Brown, J. F., Zhu, Z., Yang, L. and Merchant, J. W. (2000), Development of a global land cover characteristics database and IGBP DISCover from 1 km AVHRR. International Journal of Remote Sensing, 21, 1303-1330, doi: 10.1080/014311600210191.

Manktelow, P. T., Carslaw, K. S., Mann, G. W. and Spracklen, D. V. (2010), The impact of dust on sulfate aerosol, CN and CCN during an East Asian dust storm. Atmospheric Chemistry and Physics, 10, 365-382, doi: 10.5194/acp-10-365-2010.

Martin, M., Dash, P., Ignatov, A., Banzon, V., Beggs, H., Brasnett, B., Cavula, J.-F., Cummings, J., Donlon, C., Gentemann, C., Grumbine, R., Ishizaki, S., Maturi, E., Reynolds, R. W. and Roberts-Jones, J. (2012), Group for High Resolution Sea Surface Temperature (GHRSST) analysis fields inter-comparisons. Part 1: A GHRSST multi-product ensemble (GMPE). Deep Sea Research Part II: Topical Studies in Oceanography, 77-80, 21-30, doi: 10.1016/j.dsr2.2012.04.013.

Martinez, M. A., Ruiz, J. and Cuevas, E. (2009), Use of SEVIRI images and derived products in a WMO Sand and dust Storm Warning System. IOP Conference Series: Earth and Environmental Science, 7, 012004, doi: 10.1088/1755-1307/7/1/012004.

Martinez Avellaneda, N. M., Serra, N., Minnett, P. J. and Stammer, D. (2010), Response of the eastern subtropical Atlantic SST to Saharan dust: A modeling and observational study. Journal of Geophysical Research, 115, C08015, doi: 10.1029/2009JC005692.

Miller, S. D., Straka III, W., Mills, S. P., Elvidge, C. D., Lee, T. F., Solbrig, J., Walther, A., Heidinger, A. K. and Weiss, S. C. (2013), Illuminating the Capabilities of the Suomi National Polar-Orbiting Partnership (NPP) Visible Infrared Imaging Radiometer Suite (VIIRS) Day/Night Band. Remote Sensing, 5, 6717-6766, doi: 10.3390/rs5126717.

Miller, R. L. (2012). Adjustment to radiative forcing in a simple coupled ocean-atmosphere model. Journal of Climate, 25, 7802-7821, https://doi.org/10.1175/JCLI-D-11-00119.1.

Myhre, G., Grini, A., Haywood, J. M., Stordal, F., Chatenet, B., Tanré, D., Sundet, J. K. and Isaksen, I. S. A. (2003), Modeling the radiative impact of mineral dust during the Saharan Dust Experiment (SHADE) campaign. Journal of Geophysical Research, 108, 8579, doi: 10.1029/2002JD002566.

NCEP (2015), NCEP GFS 0.25 Degree Global Forecast Grids Historical Archive.

Nelli, N. R., Temimi, M., Fonseca, R. M., Weston, M. J., Thota, M. S., Valappil, V. K., Branch, O., Wizemann, H.-D., Wulfmeyer, V. and Wehbe, Y. (2020) Micrometeorological measurements in an arid environment: Diurnal characteristics and surface energy balance closure. Atmospheric Research, 234, 104745, doi: 10.1016/j.atmosres.2019.104745.

Payne, R. E. (1972), Albedo of the Sea Surface. Journal of Atmospheric Sciences, 29, 959-979, doi: 10.1175/1520-0469(1972)029<0959;AOTSS>2.0.CO;2.

Prakash P.J., G. Stenchkov, S. Kalenderski, S. Osipov, H. Bangalath, The impact of dust storms on the Arabian Peninsula and the Red Sea, Atmos. Chem. Phys., 15 (2015), pp. 199-222, 10.5194/acp-15-199-2015.

Reed, K. A., Bacmeister, J. T., Huff, J. J. A., Wu, X., Bates, S. C. and Rosenbloom, N. A. (2019), Exploring the impact of dust on North Atlantic hurricanes in a high-resolution climate model. Geophysical Research Letters, 46, 1105-1112, doi: 10.1029/2018GL080642.

Remer, L. A., Kaufman, Y. J., Tanre, D., Mattoo, S., Chu, D. A., Martins, J. V., Li, R.-R., Ichoku, C., Levy, R. C., Kleidman, R. G., Eck, T. F., Vermote, E. and Holben, B. N. (2005) The MODIS Aerosol Algorithm, Products, and Validation. Journal of Atmospheric Sciences, 62(4), 947-973, doi: 10.1175/JAS3385.1.

Rodriguez-Cotto, R., Ortiz-Martinez, M. G., Rivera-Ramirez, E., Mendez, L. B., Davila, J. C. and Jimenez-Velez, B. D. (2013), African Dust Storms Reaching Puerto Rican Coast Stimulate the Secretion of IL-6 and IL-8 and Cause Cytotoxicity to Human Bronchial Epithelial Cells (BEAS-2B). Health (Irvine Calif), 5(10B), 14-28, doi: 10.4236/health.2013.510A2003.

Rontu, L., Gleeson, E., Perez, D. M., Nielsen, K. P. and Toll, V. (2020), Sensitivity of Radiative Fluxes to Aerosols in the ALADIN-HIRLAM Numerical Weather Prediction System. Atmosphere, 11(2), 205, doi: 10.3390/atmos11020205.

Journal Pre-proof

Saeed, T. M., Al-Dashti, H. and Spyrou, C. (2014), Aerosol's optical and physical characteristics and direct radiative forcing during a shamal dust storm, a case study. Atmospheric Chemistry and Physics, 14, 3751-3769, doi: 10.5194/acp-14-3751-2014.

Saleeby S.M., S.C. van den Heever, J. Bukowski, A.L. Walker, J.E. Solbrig, S.A. Atwood, Q. Bian, S.M. Kreidenweis, Y. Wang, J. Wang, S.D. Miller, 'The influence of simulated surface dust lofting and atmospheric loading on radiative forcing', Atmos. Chem. Phys., 19 (2019), pp. 10279-10301, 10.5194/acp-19-10279-2019.

Sanchez, P. A., Ahmed, S., Carre, F., Hartemink, A. E., Hempel, J., Huising, J., Lagacherie, P., McBratney, A. B., McKenzie, N. J., Mendonca-Santos, M. L., Minasny, B., Montanarella, L., Okoth, P., Palm, C. A., Sachs, J. D., Shepherd, K. D., Vagen, T.-G., Vanlauwe, B., Walsh, M. G., Winowiecki, L. A. and Zhang, G.-L. (2009), Digital soil map of the world. Science, 325, 680-681, doi: 10.1126/science.1175084.

Saidou Chaibou, A. A., Ma, X. and Sha, T. (2020), Dust radiative forcing and its impact on surface energy budget over West Africa. Scientific Reports, 10, 12236, doi: 10.1038/s41598-020-69223-4.

Schmetz, J., Pili, P., Tjemkes, S., Just, D., Kerkmann, J., Rota, S. and Ratier, A. (2002), An introduction to Meteosat Second Generation (MSG). Bulletin of the American Meteorological Society, 83, 977-992, doi: 10.1175/1520-0477(2002)083,0977:AITMSG.2.3.CO;2.

Sertel, E., Robock, A. and Ormeci, C. (2010), Impacts of land cover data quality on regional climate simulations. International Journal of Climatology, 30, 1942-1953, doi: 10.1002/joc.2036.

Satheesh, S. K. and Krishna Moorthy, K. (2005), Radiative effects of natural aerosols: A review. Atmospheric Environment, 39, 2089-2110. doi: 10.1016/j.atmosenv.2004.12.029.

Singh, C., Kumar Singh, S., Chauhan, P. and Budakoti, S. (2021), Simulation of an extreme dust episode using WRF-CHEM based on optimal ensemble approach. Atmospheric Research, 249, 105296, doi: 10.1016/j.atmosres.2020.105296.

Skamarock, W. C., Klemp, J. B., Dudhia, J., Gill, D. O., Barker, D. M., Duda, M. G., Huang, X.-Y., Wang, W. and Powers, J. G. (2008), A Description of the Advanced Research WRF Version 3. NCAR, doi: 10.5065/D68S4MVH.

Slingo, A., Ackerman, T. P., Allan, R. P., Kassianov, E. I., McFarlane, S. A., Robinson, G. J., Barnard, J. C., Miller, M. A., Harries, J. E., Russell, J. E. and Dewitte, S. (2006), Observations of the impact of a major Saharan dust storm on the atmospheric radiation balance. Geophysics Research Letters, 33, L24817, doi: 10.1029/2006GL027869.

Sokolik, I. N., Winker, D. M., Bergametti, G., Gillette, D. A., Carmichael, G., Kaufman, Y. J., Gomes, L., Schuetz, L. and Penner, J. E. (2001), Introduction to special section: Outstanding problems in quantifying the radiative impacts of mineral dust. Journal of Geophysical Research, 106, 18015-18027, doi: 10.1029/2000JD900498.

Solomos, S., Ansmann, A., Mamouri, R.-E., Binietoglou, I., Patlakas, P., Marinou, E. and Amiridis, V. (2017), Remote sensing and modelling analysis of the extreme dust storm hitting the Middle East and eastern Mediterranean in September 2015. Atmospheric Chemistry and Physics, 17, 4063-4078, doi: 10.5194/acp-17-4063-2017.

Solomos, S., Kalivitis, N., Mihalopoulos, N., Amiridis, V., Kouvaris, G., Gkikas, A., Binietoglou, I., Tsekeri, A., Kazadzis, S., Kottas, M., Pradhan, Y., Proestakis, E., Nastos, P. T. and Marenco, F. (2018), From Tropospheric Folding to Khamsin and Foehn Winds: How Atmospheric Dynamics Advanced a Record-Breaking Dust Episode in Crete. Atmosphere, 9, 240, doi: 10.3390/atmos9070240.

Su, L. and Fung, J. C. H. (2015), Sensitivities of WRF- Chem to dust emission schemes and land surface properties in simulating dust cycles during springtime over East Asia. Journal of Geophysical Research Atmosphere, 120, 11215– 11230, doi: 10.1002/2015JD023446.

Spyrou, C. (2018), Direct radiative impacts of desert dust on atmospheric water content. Aerosol Science and Technology, 52, 693-701, doi: 10.1080/02786826.2018.1449940.

Spyrou, C., Kallos, G., Mitsakou, C., Athanasiadis, P., Kalogeri, C. and Iacono, M. J. (2013), Modeling the radiative effects of desert dust on weather and regional climate. Atmospheric Chemistry and Physics, 13, 5489-5504, doi: 10.5194/acp-13-5489-2013.

Takemura, T., Egashira, M., Matsuzawa, K., Ichijo, H., O'ishi, R., & Abe-Ouchi, A. (2009). A simulation of the global distribution and radiative forcing of soil dust aerosols at the Last Glacial Maximum. Atmospheric Chemistry and Physics, 9, 3061-3073. https://doi.org/10.5194/acp-9-3061-2009.

Tanre, D., Haywood, J. M., Pelon, J., Leon, J. F., Chatenet, B., Formeti, P., Francis, P., Goloub, P., Highwood, E. J. and Myhre, G. (2003), Measurement and modeling of the Saharan dust radiative impact: overview of the SaHAran Dust Experiment (SHADE). Journal of Geophysical Research, 8574, 108(D13), 10.1029/2003JD003273.

Teixeira, J. C., Carvalho, A. C., Tuccella, P., Curci, G. and Rocha, A. (2016), WRF-Chem sensitivity to vertical resolution during a saharan dust event. Physics and Chemistry of the Earth, Parts A/B/C, 94, 188-195, doi: 10.1016/j.pce.2015.04.002.

Tewari, M., Chen, F., Wang, W., Dudhia, J., Lemone, M. A., Mitchell, K., Ek, M., Gayno, G., Wegiel, J. and Cuenca, R. H. (2004), Implementation and verification of the unified NOAH land surface model in the WRF model. 20th conference on weather analysis and forecasting / 16th conference on numerical weather prediction, 11-15, available online at https://ams.confex.com/ams/pdfpapers/69061.pdf.

Todd, M. C., Bou Karam, D., Cavazos, C., Bouet, C., Heinold, B., Baldasano, J. M., Cautenet, G., Koren, I., Perez, C., Solomon, F., Tegen, I., Tulet, P., Washington, R. and Zakey, A. (2008), Quantifying uncertainty in estimates of mineral dust flux: An intercomparison of model performance over the Bodele Depression, northern Chad. Journal of Geophysical Research, 113, D24107, doi: 10.1029/2008JD010476.

Uzan, L., Egert, S. and Alpert, P. (2018), New insights into the vertical structure of the September 2015 dust storm employing eight ceilometers and auxiliary measurements over Israel. Atmospheric Chemistry and Physics, 18, 3203-3221, doi: 10.5194/acp-18-3203-2018.

Wang J., U. Nair, S.A. Christopher (2004) GOES-8 Aerosol optical thickness assimilation in a mesoscale model: Online integration of aerosol radiative effects, J. Geophys. Res., 109 (2004), 10.1029/2004JD004827D23203.

Wang, H., Shi, G., Li, S., Li, W., Wang, B. and Huang, Y. (2006), The impacts of optical properties on radiative forcing due to dust aerosol. Advances in Atmospheric Sciences, 23, 431-441, doi: 10.1007/s00376-006-0431-5.

Wang W., J. Huang, T. Zhou, J. Bi, L. Lin, Y. Chen, Z. Huang, J. Su (2013) Estimation of radiative effect of a heavy dust storm over Northwest China using Fu–Liou model and ground measurements, Elsevier J. Quant. Spectr. Radiat. Transf., 122 (2013), pp. 114-126, 10.1016/j.jqsrt.2012.10.018.

Wang, Y., Chen, L., Xin, J. and Wang, X. (2020), Impact of the Dust Aerosol Model on the VIIRS Aerosol Optical Depth (AOD) Product across China. Remote Sensing, 12, 991, doi: 10.3390/rs12060991.

Wang, W., Mao, F., Pan, Z., Du, L. and Gong, W. (2017), Validation of VIIRS AOD through a Comparison with a Sun Photometer and MODIS AODs over Wuhan. Remote Sensing, 9, 403, doi: 10.3390/rs9050403.

Weston, M. J., M. Temimi, N. R. Nelli, R. M. Fonseca, M. S. Thota and V. K. Valappil (2020), On the Analysis of the Low-Level Double Temperature Inversion Over the United Arab Emirates: A Case Study during April 2019, IEEE Geoscience and Remote Sensing Letters, 1-5, doi: 10.1109/LGRS.2020.2972597.

Xie, X., Liu, X., Che, H., Xie, X., Wang, H., Li, J., … Liu, Y. (2018). Modeling East Asian dust and its radiative feedbacks in CAM4-BAM. Journal of Geophysical Research: Atmospheres, 123, 1079-1096. https://doi.org/10.1002/2017JD027343.

Zeng, X. and Beljaars, A. (2005), A prognostic scheme of sea surface skin temperature for modeling and data assimilation. Geophysical Research Letters, 32, L14605, doi: 10.1029/2005GL023030.

Zhao, C., Liu, X., Ruby Leung, L. and Hagos, S. (2011), Radiative impact of mineral dust on monsoon precipitation variability over West Africa. Atmospheric Chemistry and Physics, 11, 1879-1893, doi: 10.5194/acp-11-1879-2011.

Journal Pre-proof

Journal Pre-proof

The Radiative Impact of the June 2020 historical Saharan Dust Storm

Diana Francis[1*], Narendra Nelli[1], Ricardo Fonseca[1], Michael Weston[1], Cyrille Flamant[2], Charfeddine Cherif[1]

[1] Environmental and Geophysical Sciences Lab, Khalifa University, P.O. Box 127788, Abu Dhabi, UAE.

[2] CNRS and UVSQ, LATMOS, Sorbonne Universités, 75005 Paris, France.

Corresponding Author: diana.francis@ku.ac.ae

Conflict of Interest: The authors declare they don't have any conflict of interest.

Journal Pre-proof